ESD-TR-66-42

1

Solid State Research

1966

Prepared under Electronic Systems Division Contract AF 19(628)-5167 by

Lincoln Laboratory
MASSACHUSETTS INSTITUTE OF TECHNOLOGY
Lexington, Massachusetts

The work reported in this document was performed at Lincoln Laboratory, a center for research operated by Massachusetts Institute of Technology, with the support of the U.S. Air Force under Contract AF 19(628)-5167.

Distribution of this document is unlimited.

1

Solid State Research

1966

Issued 6 May 1966

Lincoln Laboratory

MASSACHUSETTS INSTITUTE OF TECHNOLOGY

Lexington, Massachusetts

ABSTRACT

This report covers in detail the solid state research work at Lincoln Laboratory for the period 1 November 1965 through 31 January 1966. The topics covered are Solid State Device Research, Optical Techniques and Devices, Materials Research, and Physics of Solids.

In order that four reports on solid state research may be issued during a calendar year, the number of this report is 1966 No. 1 rather than 1965 No. 4. There will be no report numbered 1965 No. 4.

Accepted for the Air Force
Franklin C. Hudson
Chief, Lincoln Laboratory Office

INTRODUCTION

I. SOLID STATE DEVICE RESEARCH

Laser action has been obtained at ~6900 Å in the red and ~4900 Å in the green from crystals of CdSe and CdS, respectively, bombarded by a beam of fast electrons. Mode structure has been observed in the laser spectra of both these materials, and the wavelength separation between the modes agrees very well with that calculated for the Fabry-Perot mode spacing using the known values for the refractive indices and their dispersion. In both materials, the beam current at the threshold for lasing did not change significantly between nitrogen and helium temperatures. For CdSe, the threshold current density varied from 1.5 A/cm^2 at 20 keV (the lowest electron energy at which lasing could be observed) to 0.2 A/cm^2 at 75 keV (the highest electron energy used), while for CdS, the corresponding values of threshold current were about a factor of five higher. The intensity in all samples saturated at high currents, presumably because of heating – e.g., for 50-keV electrons at about 1.6 A/cm^2 in CdSe, and 6.5 A/cm^2 in CdS. The current level at which saturation occurred increased somewhat with increasing beam voltage. For CdSe at 50 keV, a peak output power of 16 watts at 6850 Å at helium temperature and 10 watts at 6915 Å at nitrogen temperature was measured, corresponding to over-all power efficiencies of 8 and 5 percent, respectively. The observed power efficiencies in CdS were considerably lower, i.e., 0.7 percent at helium temperature and 0.3 percent at nitrogen temperature, corresponding to peak optical powers of 10 watts at 4910 Å and 4 watts at 4950 Å, respectively, with a 70-keV beam. Since there is some backscattering of the incident electrons, and the laser emission occurred in only a few small filaments, the local efficiency is presumably even higher in both materials.

Laser action has been obtained at 8300 Å from bulk GaAs pumped with radiation at 7900 Å from a $Ga(As_{0.94}P_{0.06})$ diode laser. Potentially, this technique should be very efficient in the conversion of pump power to laser radiation. The resulting decrease in heat dissipation (compared to inefficient pumping schemes) may enable the design of high-power output stages for semiconductor laser transmitters.

The resistivity of several samples of n-CdTe has been found to increase with hydrostatic pressure by factors of greater than 10^4 between 1 and 28,000 kG/cm^2 at room temperature. This change in resistivity with pressure is too large to be explained either in terms of an increase in average electron mass [either in the (000) minimum or because of electron transfer to higher mass minima] or in terms of deionization into hydrogenic or deep-lying impurities. The pressure coefficient at high pressure of 12.6×10^{-6} $eV/kG\text{-}cm^{-2}$ is very close to the pressure dependence for the separation of the (000) and (100) band minima, and suggests the interpretation of these results in terms of deionization into an impurity level associated with the higher lying (100) conduction band minimum.

II. OPTICAL TECHNIQUES AND DEVICES

Measurements of the infrared radiation emitted by GaAs in the 8300 to 9000 Å spectral region when bombarded by a high-power density electron beam suggest that this compound has potential as an intense, high-speed, high-resolution phosphor. In order to evaluate this potential, some of the cathodoluminescence characteristics of GaAs are compared to those of the P-11 phosphor. The upper limit of emission intensity that can be expected from GaAs is examined.

The search for a material that would be suitable as a coherent heterodyne detector for the 10.6-μ CO_2 laser radiation has led to a study of Mn-doped GaAs. Unfortunately, the extremely short lifetime ($\sim 10^{-13}$ sec) of the excited Mn acceptor level makes this material far more sensitive as a thermistor detector than as a photoconductor of high speed.

Experiments are reported which determine the probability distribution of the photoelectron counts for a photomultiplier illuminated by a laser slightly below or above the threshold of oscillation.

III. MATERIALS RESEARCH

In order to check the validity of x-ray scattering theory for broad-band semiconductors, the x-ray diffraction of powdered ZnSe has been studied in detail. For a number of weak lines, there are very large discrepancies between the calculated and observed intensities. This result supports the contention that neglect of overlap terms is an important source of error in the theoretical calculations.

The investigation of the transport properties of Ti_2O_3 has been continued by measuring the resistivity and Hall coefficient of single crystals containing low concentrations of nitrogen as the principal impurity. At 4.2°K, the magnetoresistance is directly proportional to the square of the magnetic field up to 170 kG, the highest field employed. The experimental results are consistent with a previously proposed model according to which mixed conduction occurs at 4.2°K, whereas hole conduction takes place at 77° and 273°K.

Optical absorption and EPR measurements have been made on electron-irradiated ruby in order to determine why the cathodoluminescence of ruby saturates and then decreases as the exciting electron beam current is increased. Preliminary results indicate that under irradiation the reaction $2Cr^{+3} \rightleftharpoons Cr^{+2} + Cr^{+4}$ is forced to the right. This could account for the decrease in cathodoluminescence, since neither Cr^{+2} nor Cr^{+4} fluoresces, and it appears that Cr^{+4} quenches the fluorescence of Cr^{+3}.

The outer-electron configuration for α-iron has been determined from the magnetization, g-factor, and symmetries of electron- and spin-density form factors. Lack of complete magnetization of the 3d bands, together with a knowledge of the magnetic ordering in Cr, CrMn and α-iron, provides information about the nature of electron-electron interactions within a band as a function of the number of electrons in the band. This information is consistent with evidence from several oxides with the perovskite structure.

IV. PHYSICS OF SOLIDS

The study of the room-temperature reflectivity of ReO_3 is continuing. Kromers-Kronig analyses have yielded the real and imaginary parts of the dielectric constant, the effective number of electrons, and the loss function.

The investigation of the layer compound GaSe has been extended. The magnetoabsorption spectrum in the Voigt configuration was found to be isotropic for the magnetic field in the c-plane and radiation along the c-axis. Absorption measurements in crossed electric and magnetic fields have been initiated. Electroluminescence, as well as magnetic effects on the electroluminescence, has been observed.

Two series of magnetoreflection oscillations have been observed in HgTe, corresponding to two sets of transitions; these results are consistent with a gray tin-like band structure for HgTe.

An extension of the previous magnetoreflection studies in bismuth has not only corroborated the former work, but has also revealed additional structure; in particular, a new series of oscillations has been observed with an energy gap $E_g = 0.169$ eV which corresponds to one of the gaps reported by Esaki from electron tunneling experiments.

In collaboration with Professor A. Javan of the M. I. T. Physics Department, the low quantum number interband Landau level transitions in graphite are being studied with a high-resolution magnetospectrometer using a neon gas laser source. Substantial improvement has been achieved over conventional sources in resolution, line shape and signal-to-noise ratio.

A best fit of the experimental derivative of the microwave surface magnetoabsorption at 70 GHz in p-type PbSe with a classical skin effect theory, including a finite relaxation time, has been carried out. The values of transverse effective mass $m_t = (0.0465 \pm 0.0015)\, m_o$ and anisotropy ratio $K \equiv m_\ell/m_t = 1.8 \pm 0.2$ required for this fit are in satisfactory agreement with the results of Shubnikov-de Haas measurements.

The energy band structure of TiO in the tight-binding theory has been used in an interpolation scheme to approximate the energy bands determined by APW calculations.

The Fermi surface of thulium metal has been determined from a nonrelativistic APW energy band calculation. The computed Fermi surface allows an explanation of the c-axis resistivity anomaly observed in the heavy rare-earth metals at the onset of long range periodic magnetic order.

A Brillouin-Wigner perturbation calculation and a variational calculation have been made for the energy of the $n = 1$ Landau level of a polaron in a magnetic field. The calculations show that as the magnetic field increases, the energy deviates markedly from the usual linear behavior with H and approaches a limiting value.

Measurements of the temperature dependence of 70-GHz acoustic waves in quartz have now been extended to include transverse waves. The T^4 dependence which was previously found for the longitudinal waves is obtained also for the transverse mode, down to 10°K.

Comparative data have been obtained by pulse echo techniques of the performance of insulating piezoelectric CdS film transducers relative to other forms of acoustic excitation in the frequency range from 14 MHz to 70 GHz. The CdS transducers have superior insertion loss characteristics over other common modes of excitation up to 9 GHz, comparable characteristics at 24 GHz, and poorer efficiencies at 70 GHz (on z-cut quartz).

A calculation has been initiated for the classical ground spin state of a magnetic spinel with nonmagnetic ions on the A-sites. Examples of this case are ferromagnetic $CdCr_2Se_4$ and antiferromagnetic $ZnCr_2Se_4$. Magnetic resonance measurements at X-band have begun on the ferromagnetic chalcogenides whose DC magnetic properties had previously been investigated. First results have been obtained in polycrystalline $CdCr_2S_4$ on the line width and g-factor as a function of temperature over the ferromagnetic region as well as the paramagnetic region.

Relations have been obtained between the coefficients of higher-order temperature-dependent terms in the spin-wave dispersion relations. Explicit expressions for these coefficients have been obtained for the case of a Heisenberg model.

Two recent theories of the symmetry restrictions on transport coefficients for magnetic materials have been compared, and it has been shown that one of these is inconsistent with the existence of the anomalous Hall effect.

High-power ruby laser scattering experiments in quartz have been extended to low temperatures. Compared with room temperature, the stimulated Brillouin threshold is only slightly lower, while there is a significant reduction in the stimulated Raman threshold. A number of combination lines belonging to different vibrational modes of the quartz lattice have been observed.

Incoherent second harmonic scattering of ruby laser light in water has been studied as the temperature is lowered toward the freezing point. The scattering increases roughly linearly with decreasing temperature below room temperature.

Possible origins of the nonlinear dependence of index of refraction on field strength, which can give rise to self-focusing or beam-trapping effects, continue to be investigated. It is pointed out that close to an atomic resonance, the real part of the susceptibility can be a strong function of power level because of saturation.

CONTENTS

ORGANIZATION

SOLID STATE DIVISION

A. L. McWhorter, *Head*
P. E. Tannenwald, *Associate Head*
M. J. Hudson, *Assistant*
E. P. Warekois
D. T. Stevenson*
T. C. Harman†

SOLID STATE THEORY

H. J. Zeiger, *Leader*
M. M. Litvak, *Assistant Leader*

Argyres, P. N.
Dresselhaus, G. F.
Houghton, B. H.*
Kaplan, T. A.
Kleiner, W. H.
Larsen, D. M.
Mason, V. J.
Mason, W. C.
Rawson, N. B.*
Stanley, H. E.*
Trent, P. H.
Van Zandt, L. L.

OPTICS AND INFRARED

R. H. Kingston, *Leader*
R. J. Keyes, *Assistant Leader*

Bates, D. H.
Bostick, H. A.
Carbone, R. J.
Dennis, J. H.
Freed, C.
Longaker, P. R.
McGowan, J.
Walters, E.
Zimmerman, M. D.

ELECTRONIC MATERIALS

J. B. Goodenough, *Leader*
J. M. Honig, *Associate Leader*
A. J. Strauss, *Assistant Leader*

Andrews, H. I.‡
Arnott, R. J.
Bachner, F. J.‡
Banus, M. D.
Brebrick, R. F.
Button, M. J.
Cornwell, J. C.
Delaney, E. J.
Ehlers, H. H.
Fahey, R. E.
Farrell, L. B.
Ferretti, A.
Finn, M. C.
Fischler, S.
Germann, R. W.
Hilsenrath, S.
Kafalas, J. A.
LaFleur, W. J.
Lavine, M. C.*
Longo, J. M.
Newman, W. A.
O'Connor, J. R.
Owens, E. B.
Paladino, A. E.
Plonko, M. C.
Pollard, E. R.‡
Rabbio, M. A.
Raccah, P. M.
Reed, T. B.†
Ridgley, D. H.
Roddy, J. T.
Siuta, V. P.‡
Sohn, J. B.

SOLID STATE PHYSICS

J. G. Mavroides, *Leader*
G. B. Wright, *Assistant Leader*

Bermon, S.
Burke, J. W.
Carman, R. L.*
Dickey, D. H.
Dresselhaus, M. S.
Dwight, K., Jr.
Feinleib, J.
Feldman, B.
Fulton, M. J.
Groves, S. H.
Halpern, J.
Johnson, E. J.
Kernan, W. C.
Kolesar, D. F.
Krag, W. E.
Mastromattei, E. L.
Menyuk, N.
Parker, C. D.
Perry, F. H.
Schlossberg, H. R.‡
Scouler, W. J.
Stickler, J. J.‡
Strahm, N. D.‡
Thaxter, J. B.
Weber, R.
Weinberg, D. L.

APPLIED PHYSICS

R. H. Rediker, *Leader*
J. O. Dimmock, *Associate Leader*
I. Melngailis, *Assistant Leader*

Butler, J. F.
Calawa, A. R.
Carter, F. B.
Caswell, F. H.
Clough, T. F.
Donaldson, P. L.
Foyt, A. G.
Grant, C. R.
Hinkley, E. D.
Hurwitz, C. E.
Lindley, W. T.
McPhie, J. M.
Mooradian, A.
Nill, K. W.‡
Palermo, J. S.
Phelan, R. J., Jr.
Quist, T. M.
Sullivan, F. M.
Walpole, J. M.‡
Ward, J. H. R., III
Wolfe, C. M.
Womac, J.‡
Youtz, P.

---

*Part Time
†Leave of Absence
‡Research Assistant

REPORTS BY AUTHORS ENGAGED IN SOLID STATE RESEARCH

15 November 1965 through 15 February 1966

PUBLISHED REPORTS

Journal Articles*

JA No.			
2376	Cyclotron Resonance: (Diamagnetic Resonance)	G. F. Dresselhaus	Encyclopedia of Physics, R. M. Besancon, ed. (Reinhold, New York, 1966)
2410	Diamagnetism	J. B. Goodenough	
2501	Galvano-Thermomagnetic Phenomena and the Figure of Merit in Bismuth. II. Survey of Experimental Data and Calculation of Device Parameters	T. C. Harman J. M. Honig L. M. Jones†	Adv. Energy Conversion 5, 183 (1965), DDC 628559
2520	The Relation of the Electrical Conductivity in Single Crystals of Rhenium Trioxide to the Conductivities of Sr_2MgReO_6 and Na_xWO_3	A. Ferretti D. B. Rogers J. B. Goodenough	J. Phys. Chem. Solids 26, 2007 (1965), DDC 630364
2530	Preparation and Paramagnetism of the Rare Earth Trifluorides	S. Kern P. M. Raccah	J. Phys. Chem. Solids 26, 1625 (1965), DDC 624722
2580	Particle Sizes of Clay Minerals by Small-Angle X-Ray Scattering	R. J. Arnott	Am. Mineralogist 50, 1563 (1965), DDC 630376
2597	The Bohr-Sommerfeld Quantization Rule and the Weyl Correspondence	P. N. Argyres	Physics 2, 131 (1965), DDC 626877
2599	High Field Magnetoabsorption of the Indirect Transition Exciton in Germanium at 1.7°K	J. Halpern B. Lax	J. Phys. Chem. Solids 27, 111 (1966), DDC 630372
2600	Partial Pressure of Se_2 and Optical Density of Selenium Vapor in the Visible and Ultraviolet	R. F. Brebrick	J. Chem. Phys. 43, 3031 (1965), DDC 626893
2609	deHaas-van Alphen Effect in Pyrolytic and Single Crystal Graphite	S. J. Williamson† S. Foner† M. S. Dresselhaus	Phys. Rev. 140, A1429 (1965)

* Reprints available.

† Author not at Lincoln Laboratory.

Reports

JA No.			
2610	Pressure of Hg and Selenium Over HgSe(c) from Optical Density Measurements	R. F. Brebrick	J. Chem. Phys. 43, 3846 (1965)
2622	Towards a Theory of the Anomalous Thermoelectric Effect in Magnetically Dilute Alloys	L. L. Van Zandt A. W. Overhauser*	Phys. Rev. 141, 583 (1966)
2626	Photocurrent Spectrum and Photoelectron Counts Produced by a Gaseous Laser	C. Freed H. A. Haus*	Phys. Rev. 141, 287 (1966)
2641	Magnetic and Electric Properties of ReO_2: Theoretical	J. B. Goodenough P. Gibart* J. Brenet*	Compt. rend. 261, 2331 (1965)
2642	Solution Regrowth of Planar InSb Laser Structures	I. Melngailis A. R. Calawa	J. Electrochem. Soc. 113, 58 (1966), DDC 630373
2644	The Gunn Effect in Polar Semiconductors	A. G. Foyt A. L. McWhorter	IEEE Trans. Electron Devices ED-13, No. 1 (1966)
2653	Resistance Heated Crystal Puller for Operation at 2000°C	T. B. Reed R. E. Fahey	Rev. Sci. Instr. 37, 59 (1966)
2684	Self-Focusing of Optical Beams	P. L. Kelley	Phys. Rev. Letters 15, 1005 (1965), DDC 628563
2697	Bulk GaAs Microwave Amplifiers	A. G. Foyt T. M. Quist	IEEE Trans. Electron Devices ED-13, No. 1 (1966)
2708	Photoelectron Statistics Produced by a Laser Operating Below the Threshold of Oscillation	C. Freed H. A. Haus*	Phys. Rev. Letters 15, 943 (1965)
2735	Fermi Surface, Magnetic Ordering and Electrical Properties of Rare-Earth Metals	A. J. Freeman* J. O. Dimmock R. E. Watson*	Phys. Rev. Letters 16, 94 (1966)
2743	Evidence for Impurity States Associated with High-Energy Conduction Band Extrema in n-CdTe	A. G. Foyt R. S. Halsted* W. Paul*	Phys. Rev. Letters 16, 55 (1966)
MS No.			
843A	Magnetic Ordering in Heisenberg Magnets	T. A. Kaplan	The Molecular Designing of Materials and Devices, A. R. Von Hippel, ed. (M.I.T. Press, Cambridge, 1965)
900	Properties Imparted by d Electrons	J. B. Goodenough	

* Author not at Lincoln Laboratory.

MS No.			
932	Electrons and Holes in Semiconductors	H.J. Zeiger	The Molecular Designing of Materials and Devices, A.R. Von Hippel, ed. (M.I.T. Press, Cambridge, 1965)
1110A	Principles of Injection Lasers	R.H. Rediker	Optical and Electro-Optical Information Processing (M.I.T. Press, Cambridge, 1965)
1339	Amplitude Noise in Gas Lasers Below and Above the Threshold of Oscillation	C. Freed H.A. Haus*	Physics of Quantum Electronics, P.L. Kelley, B. Lax and P.E. Tannenwald, eds. (McGraw-Hill, New York, 1966)
1343	Sum and Difference Frequency Generation in Gases and Liquids	P.N. Butcher* W.H. Kleiner P.L. Kelley H.J. Zeiger	
1396	Magneto-Emission Studies of PbS, PbTe, and PbSe Diode Lasers	J.F. Butler A.R. Calawa	
1397	Laser Emission by Optical Pumping of Semiconductors	R.J. Phelan, Jr.	
1398	Multiple Stimulated Brillouin Scattering in Solids	P.E. Tannenwald	
1399	Plasmon Scattering of Light and Stimulated Emission of Plasmons in Solids	A.L. McWhorter	
1447	Semiconductor Bulk Injection Lasers	I. Melngailis	NEREM Record 7, 240 (1965)

* * * * *

UNPUBLISHED REPORTS

Journal Articles

JA No.			
2508	Photographic Emission as Ion Detectors in Quantitative Mass Spectrography	E.B. Owens	Accepted as Chapter 3 in Mass Spectrometric Analysis of Solids (Elsevier, New York)
2570	Space-Time Symmetry of Transport Coefficients	W.H. Kleiner	Accepted by Phys. Rev.

* Author not at Lincoln Laboratory.

Reports

JA No.			
2613A	Automatic Potentiometric EDTA and Redox Titrations for Determinations of Stoichiometry	M.C. Gardels J.C. Cornwell	Accepted by Anal. Chem.
2620	A Volumetric Determination of Arsenic and Antimony in Mixed Manganese Arsenide, Antimonide and Phosphide Compounds	E.R. Whipple* D.H. Ridgley	Accepted by Anal. Chim. Acta
2625	Cyclotron Resonance of Piezoelectric Polarons	D.M. Larsen	Accepted by Phys. Rev.
2640	Discussion of "Theory of Nonequilibrium Thermodynamics with Application to the Transport Processes in a Solid" by M.R. El-Saden	J.M. Honig	Accepted by Trans. ASME
2661	Observation of Interband Transitions in Cd_3As_2	E.D. Haidemenakis* J.G. Mavroides M.S. Dresselhaus D.F. Kolesar	Accepted by Solid State Commun.
2667	Four-Probe Device for Accurate Measurement of the Temperature Dependence of Electrical Resistivity on Small, Irregular-Shaped Single Crystals	R.W. Germann D.B. Rogers	Accepted by Rev. Sci. Instr.
2668	On the Polaron Energy Spectrum	D.M. Larsen	Accepted by Phys. Rev.
2670	Remarks on: "An Explanation of the High Cation Vacancy Concentration and p-Type Conductivity in Semiconductors Containing a Multivalent Metal in Its Lowest Valence State"	R.F. Brebrick	Accepted by J. Phys. Chem. Solids
2672	Pseudo-Binary InSb-InTe System	A.J. Strauss M.D. Banus M.C. Finn	Accepted by J. Electrochem. Soc.
2698	Structure of Equations Specifying Operating Characteristics of Energy Converters Constructed of Anisotropic Materials	J.M. Honig T.C. Harman	Accepted by Adv. Energy Conversion
2731	Comparative Data on CdS Transducers from 14 Mc/s to 70 Gc/s	R. Weber	Accepted by Proc. IEEE

* Author not at Lincoln Laboratory.

JA No.			
2736	The Augmented Plane Wave Method and the Electronic Properties of Rare-Earth Metals	A.J. Freeman* J.O. Dimmock R.E. Watson*	Accepted as chapter in Theory of Atoms, Molecules and Solids (Academic Press, New York)
2757	Electron Beam Pumped Lasers of CdSe and CdS	C.E. Hurwitz	Accepted by Appl. Phys. Letters

Meeting Speeches†

MS No.			
1036F	The Band Structure of Semimetals from Magnetoreflection Experiments	M.S. Dresselhaus	Colloquium, Tufts University, 19 November 1965
1036G-I	Magnetoreflection Studies in Semimetals	M.S. Dresselhaus	Colloquium, University of Utah, 16 December 1965; Colloquium, University of California, 17 December 1965; Seminar, Ford Motor Company Scientific Laboratory, Dearborn, Michigan, 10 January 1966
1243I-J	Recent Advances in Semiconductor Lasers	R.H. Rediker	Seminar, National Research Laboratory, Washington, D.C., 6 December 1965; Seminar, Purdue University, 17 December 1965
1415	Designing of Multi-Region Pressure Vessels Using Maximum Shear Theory	A.R. Leyenaar J.A. Kafalas	ASME Symposium, Chicago, Illinois, 7 November 1965
1447A	Semiconductor Bulk Injection Lasers	I. Melngailis	ILO Symposium, M.I.T., 14 December 1965
1528	Transferred Electron Effects in n-GaAs	A.G. Foyt	
1459	Ferromagnetism in $CdCr_2Se_4$ and $CdCr_2S_4$	N. Menyuk K. Dwight R.J. Arnott A. Wold*	11th Annual Conference on Magnetism and Magnetic Materials, San Francisco, California, 16-19 November 1965
1463	Reduced Manganese Moment in Manganese Chromite	K. Dwight N. Menyuk J. Feinleib A. Wold*	

* Author not at Lincoln Laboratory.

† Titles of Meeting Speeches are listed for information only. No copies are available for distribution.

Reports

MS No.			
1464	Single Crystal Growth and Properties of the Perovskites $LaVO_3$ and YVO_3	D.B. Rogers A. Ferretti D.H. Ridgley R.J. Arnott J.B. Goodenough	11th Annual Conference on Magnetism and Magnetic Materials, San Francisco, California, 16-19 November 1965
1466	Electronic Band Structure, Fermi Surface and Magnetic Properties of Palladium Metal	A.J. Freeman* J.O. Dimmock A.M. Furdyna*	
1474	Temperature Variation of the Spin-Wave Dispersion Relation	R. Weber P.E. Tannenwald	
1475	A Covalency Criterion for Localized vs Collective Electrons in Oxides with the Perovskite Structure	J.B. Goodenough	
1477	Crystallographic Study of Several Chromium Spinels	P.M. Raccah R.J. Bouchard* A. Wold*	
1466A	Electronic Band Structure, Fermi Surface and Magnetic Properties of Palladium Metal	A.J. Freeman* J.O. Dimmock A.M. Furdyna*	International Symposium on Quantum Theory of Atoms and Molecules and Solid State Physics, Sanibel Island, Florida, 19-22 January 1966
1517A	The Symmetry of Hartree-Fock Ground States	T.A. Kaplan W.H. Kleiner	
1475B	A Covalency Criterion for Ligand-Field vs Band Electrons in Oxides with the Perovskite Structure	J.B. Goodenough	Seminar, Brown University, 10 December 1965
1486	Quantitative Evaluation of Mass Spectra of Solids	E.B. Owens	Eastern Analytical Symposium, New York, 19 November 1965
1492B	The Gunn Effect	A.L. McWhorter	Colloquium, Center for Materials Science and Engineering, M.I.T., 19 November 1965
1492C	Transferred Electron Effects in Polar Semiconductors	A.G. Foyt A.L. McWhorter	IEEE, Electron Devices Meeting, Waltham, Massachusetts, 20 January 1966
1494	Millimeter Wave Phonon Generation, Propagation and Attenuation	P.E. Tannenwald J.B. Thaxter	Ultrasonics Symposium, Boston, 1-4 December 1965
1532	9 Gc Magnetoacoustic Measurements on InSb	K.W. Nill A.L. McWhorter	

* Author not at Lincoln Laboratory.

MS No.			
1497A	Time Inversion and Transport Coefficients for Magnetic Crystals	W.H. Kleiner	Seminar, Watertown Arsenal, Watertown, Massachusetts, 22 November 1965
1509A	Electrical Properties of Metal Oxides	J.M. Honig	Colloquium, Pennsylvania State University, 14 January 1966
1512	Fourier Expansion for Energy Bands in a Periodic Solid	G.F. Dresselhaus M.S. Dresselhaus	American Physical Society, Los Angeles, California, 20-22 December 1965
1512A	Fourier Expansion for Energy Bands in a Periodic Solid	G.F. Dresselhaus	Colloquium, University of California, 17 December 1965
1529	Electron Recombination in Laser-Produced Hydrogen Plasma	M.M. Litvak	Seminar, M.I.T., 19 November 1965
1530	Stimulated Raman Scattering and Beam Trapping	H.J. Zeiger	Colloquium, Yeshiva University, New York, 18 November 1965; Colloquium, Westinghouse Electric Company, Pittsburgh, Pennsylvania, 16 December 1965
1531	Light Scattering from Spin Fluctuations in Ferromagnets	M.M. Litvak H.J. Zeiger	
1534	Refractive-Index Changes in Absorbing Media by a Pulsed Laser Beam	P.R. Longaker M.M. Litvak	
1535	High Resolution Magneto-spectroscopy of Graphite Using an Infrared Laser Source	P.R. Schroeder* A. Javan* M.S. Dresselhaus J.G. Mavroides	American Physical Society, New York, 26-29 January 1966
1536	Magnetoreflection in Bismuth	M.S. Maltz M.S. Dresselhaus	
1565	The Magnon Dispersion Relation from Spin-Wave Resonance	P.E. Tannenwald	
1582	Electron Density Measurements from Stark Linewidths in an Argon Laser	R.J. Carbone M.M. Litvak	
1540	Calculations of Electronic Energy Bands in Solids	J.O. Dimmock	Colloquium, University of Massachusetts, 22 November 1965

* Author not at Lincoln Laboratory.

Reports

MS No.			
1544	Theory of Electromagnetic Field Measurement and Photo-electron Counting	P.L. Kelley	Seminar, Yale University, 3 December 1965
1545A, B	Light Beam Self-Focusing in Nonlinear Media	P.L. Kelley	Seminar, Colorado State University, 8 December 1965; Seminar, Special Weapons Laboratory, Kirtland Air Force Base, Albuquerque, New Mexico, 9-10 December 1965
1556	Structural and Electronic Aspects of the Beta-Tungsten Structure Compounds Nb_3Sn, Nb_3Al and Nb_3Sb as Applied to Superconductivity	H.C. Gatos F.J. Bachner	ILO Symposium, M.I.T., 19 January 1966
1574	Amplification and Gunn Oscillation in "Two-Valley" Semiconductors	A.G. Foyt	International Solid-State Circuits Conference, Philadelphia, Pennsylvania, 10 February 1966
1593	CW Amplification and Gunn Oscillation in GaAs	T.M. Quist A.G. Foyt	IEEE, Active Microwave Effects in Bulk Semiconductors Conference, New York, 3-4 February 1966
1597	Admittance of GaAs Transferred-Electron Amplifier	A.L. McWhorter	
1595	Interband Oscillatory Magneto-Optical Absorption and Faraday Rotation in Semiconductors	J. Halpern	Seminar, Lowell Technological Institute, 9 February 1966

I. SOLID STATE DEVICE RESEARCH

A. ELECTRON BEAM PUMPED CdSe LASER†

Laser oscillations have been obtained in CdSe bombarded by a beam of fast electrons. Peak output power in the red (6800 to 6900 Å) in excess of 10 W with a power efficiency of better than 5 percent at both liquid helium and liquid nitrogen temperatures has been measured. Although electron beam excitation has been employed previously to pump several other semiconductors,[1] this is the first report of a high-efficiency, visible laser obtained with this technique.

Laser samples were prepared from high-purity, single-crystal, vapor-grown platelets of CdSe. The optical cavity was formed by cleaving along two parallel $(10\bar{1}0)$ faces, which were normal to the surface of the platelet and parallel to the c-axis. The width of the samples, i.e., the dimensions of the optical cavity, varied from about 75 to 500 μ, while all were about 1 mm long and 5 to 10 μ thick. One of the cavity faces was made reflecting with an evaporated layer of aluminum, and the samples were then attached to the copper cold finger of a dewar with vacuum grease. The electron beam of approximately 0.5-mm diameter was incident on the platelet surface, and the radiation was emitted normal to the beam from the unsilvered cavity face. Current was supplied in 100- to 200-nsec pulses at a repetition rate of 60/sec.

Emission spectra of a CdSe sample near liquid helium temperature below and above the laser threshold are shown in Fig. I-1(a-b). The spontaneous line centered at 6800 Å corresponds to the intense emission line observed by others in photoluminescence experiments,[2,3] and has been attributed to an exciton-ionized acceptor complex.[2] Above threshold, the Fabry-Perot mode structure of the laser line is observed, as in Fig. I-1(b). Note the expanded wavelength scale and the hundredfold increase in peak intensity over that of the spontaneous line. The laser modes for the same sample near liquid nitrogen temperature are shown in Fig. I-2. To calculate the expected Fabry-Perot mode spacing, we use the usual formula $\Delta\lambda = \lambda_o^2/2\ell(n_o - \lambda_o dn/d\lambda)$, where λ_o is the photon wavelength, ℓ is the cavity length, n_o is the index of refraction, and $dn/d\lambda$ is the dispersion, which for CdSe constitutes a large correction. From the results of Parsons, et al.[4] for n vs λ in CdSe, we obtain $n_o = 2.79$ and $dn/d\lambda = -5 \times 10^{-4}$ Å^{-1} at 6845 Å and 4.2°K, and $n_o = 2.75$ and $dn/d\lambda = -5 \times 10^{-4}$ Å^{-1} at 6915 Å and 77°K. For the cavity length of 230 μ, the calculated mode spacings are 1.6 Å at 4.2°K, and 1.7 Å at 77°K. These values are in good agreement with the average spacings of 1.4 and 1.8 Å for the spectra shown in Figs. I-1(b) and I-2, respectively. The spontaneous and laser emissions at both temperatures are polarized with $E \perp C$, as expected, since the transition with this polarization is reported[2] to be the most intense.

The beam current at the threshold for lasing was approximately the same at both nitrogen and helium temperatures, and varied from about 1.5 A/cm^2 at 20 keV (the lowest electron energy at which lasing could be observed), to about 0.2 A/cm^2 at 75 keV (the highest electron energy used). The intensity in all samples saturated at high current, e.g., at about 1.6 A/cm^2 at 50 keV,

† The work described in this section was supported in part by the AF Avionics Laboratory Director's Fund, Item Nr. 65-86.

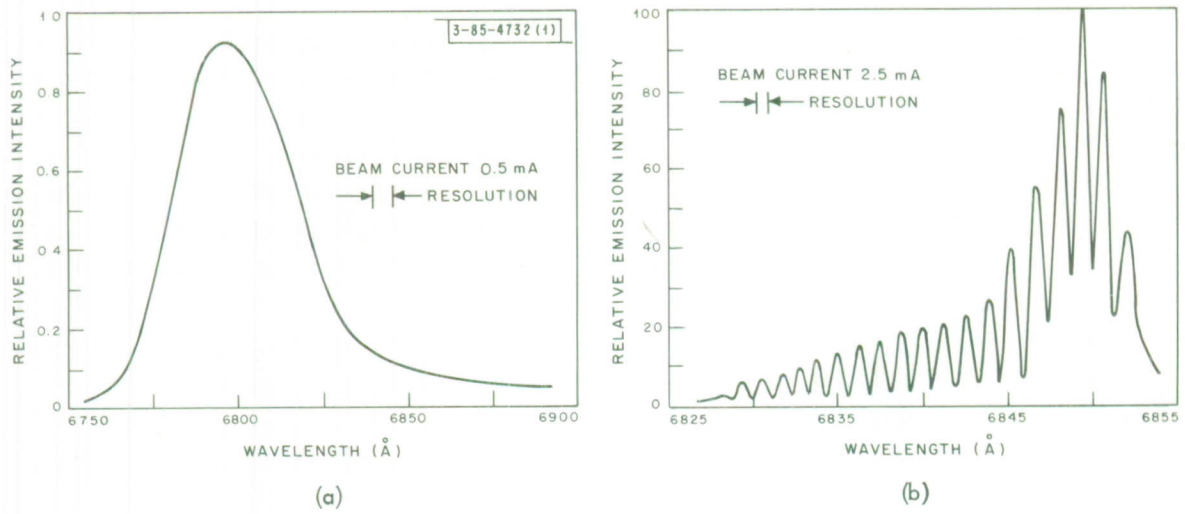

Fig. I-1. Emission spectra from electron beam pumped CdSe laser near liquid helium temperature: (a) below laser threshold (0.5-mA beam current), and (b) above laser threshold (2.5-mA beam current). Electron energy is 40 keV. Sample dimensions are 230 $\mu \times 7\ \mu \times 1$mm, the first dimension being cavity length. Note that emission intensity scale in (b) is 100 times larger in absolute magnitude than that in (a).

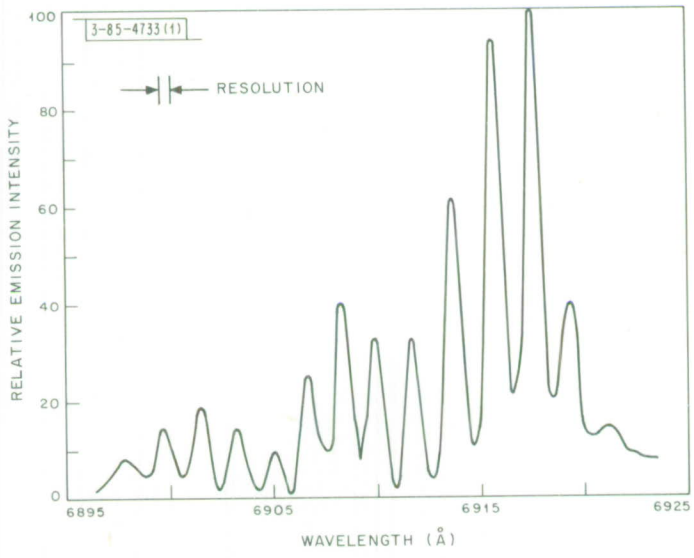

Fig. I-2. Emission spectrum for electron beam pumped CdSe laser near liquid nitrogen temperature. Electron energy is 35 keV and beam current is 3 mA. Sample dimensions are same as for Fig. I-1.

presumably because of heating. The current level at which saturation occurred, however, increased somewhat with increasing beam voltage. This is reasonable since the electron penetration depth, and therefore the active volume, increases approximately as the 1.5 power of the electron energy,[5,6] while the input power increases linearly. The gross heating of the sample by the electron beam is evident from the shift of the emission wavelength with increasing current, as seen by comparing Figs. I-1(a) and (b). From the published measurements[2] of the shift of the spontaneous peak with temperature, it is estimated that the actual sample temperatures for the laser spectra of Figs. I-1(b) and I-2 may be as high as 40° and 100°K, respectively. In taking these spectra it was, in fact, necessary to sample in time the output pulse of the photomultiplier detector with the 0.35-nsec wide time "window" of a sampling oscilloscope to minimize the spectral shift and consequent blurring of the modes caused by heating during the pulse.

We have also observed spatial diffraction patterns in the laser emission; however, these are generally complex due to the existence of several filaments lasing simultaneously and many modes per filament. For 40-keV electrons, the observed pattern for what was believed to be single filament emission gave a beam angle of about 10°. This corresponds to an emitting area 5 μ in diameter and is thus consistent with the penetration depth of 40-keV electrons.[5,6]

The peak output power at saturation increased with increasing beam voltage up to about 50 keV and remained constant thereafter. At this voltage and the saturation current of 4 mA (1.6 A/cm^2), the peak optical power obtained from a sample with a 500-μ cavity length was approximately 16 W at helium temperature and 10 W at nitrogen temperature. This corresponds to over-all power efficiencies of 8 and 5 percent, respectively, which is more than an order of magnitude higher than that observed in electron beam pumped CdS lasers (see Sec. I-B). Since the laser emission took place in only a few small filaments, the local efficiency is presumably even higher.

C. E. Hurwitz

B. ELECTRON BEAM PUMPED CdS LASER†

Basov and coworkers[7,8] have reported directionality, superlinearity, and line narrowing of the photon emission from CdS crystals excited by a beam of fast electrons and, recently, Benoit à la Guillaume and Debever[9] reported laser mode structure and directionality at 4.2° and 20°K with this method of excitation. We have independently obtained laser oscillations with well-defined cavity modes and spatial diffraction patterns in electron beam pumped CdS at 4.2°K and also at 77°K. In addition, we have measured a peak output power of 10 W at 4910 Å with an efficiency of better than 0.5 percent.

Laser samples were made from high-purity, single-crystal, vapor-grown platelets of CdS. The geometry, preparation, and mounting of the samples, and the experimental arrangements are as described in Sec. I-A.

The emission spectra shown in Fig. I-3 for three different beam currents clearly show the onset and development of laser action in a CdS sample near helium temperature. Note the rapid increase of emission intensity with a small increase in current and the formation of well-defined

† The work described in this section was supported in part by the AF Avionics Laboratory Director's Fund, Item Nr. 65-86.

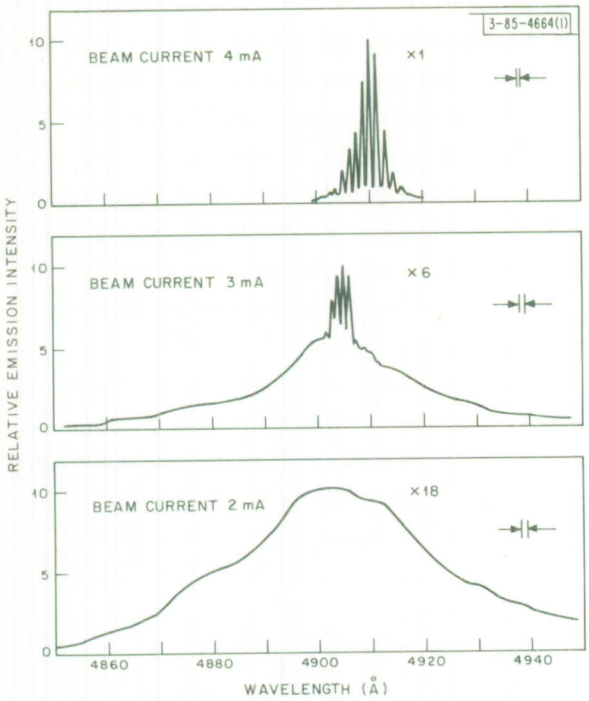

Fig. I-3. Emission spectra from electron beam pumped CdS at liquid helium temperature below laser threshold (spontaneous line), at threshold, and well above threshold. Sample dimensions are 42 μ × 17 μ × 1 mm, the first dimension being cavity length. Beam energy is 40 keV. Note multiplicative factors which have been applied to magnitudes of emission intensities.

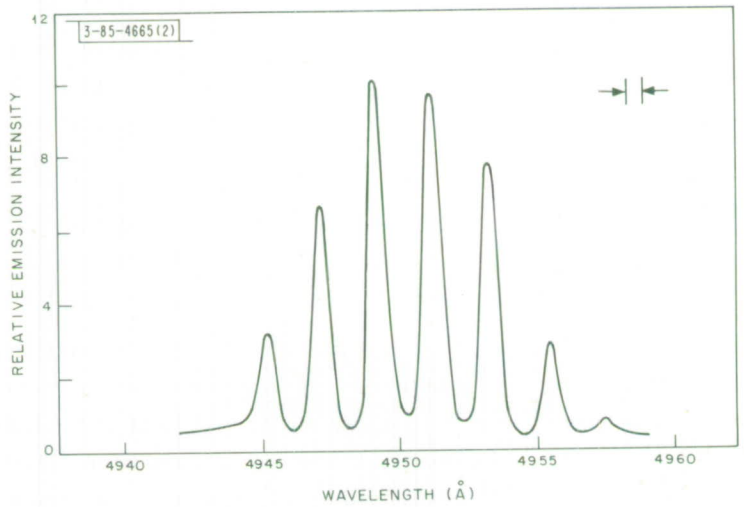

Fig. I-4. Emission spectrum from electron beam pumped CdS laser at liquid nitrogen temperature showing cavity modes. Electron beam energy 40 keV and beam current 7 mA. Sample dimensions are same as for Fig. I-3.

cavity modes. The spontaneous line, which for these samples was by far the most intense line in an otherwise complicated spectrum typical of CdS, is most probably the so-called I_1 line of CdS, which at 4.2°K is observed[10,11] at 4888 Å, and which has been associated with an exciton bound to a neutral acceptor.[10] Both the spontaneous and laser emission are polarized with E⊥C, as expected, since the I_1 transition is active only for this polarization.[10] The laser modes at liquid nitrogen temperature are shown on an expanded scale in Fig. I-4. At both temperatures there was considerable heating of the samples by the electron beam, as evidenced in Fig. I-3 by the shift of the spectral peak with increasing current. The time-resolved spectroscopic technique described in Sec. I-A was employed to minimize the transient, thermally induced spectral shift of individual modes during the pulse.

In calculating the expected Fabry-Perot mode spacing we must, as in the case of CdSe, take into account the very large dispersion $dn/d\lambda$. From the detailed results of Langer[12] for n vs λ in CdS, we obtain $n_o = 2.88$ and $dn/d\lambda = -3.64 \times 10^{-3}$ Å^{-1} at 4910 Å and 4.2°K, and $n_o = 2.85$ and $dn/d\lambda = -2.20 \times 10^{-3}$ Å^{-1} at 4950 Å and 77°K. For the cavity length of 42 μ, the usual formula yields mode spacings of 1.38 Å at 4.2°K, and 2.13 Å at 77°K. These values are in excellent agreement with the average spacings of 1.35 and 2.15 Å for the spectra shown in Figs. I-3 and I-4, respectively.

The threshold characteristics and the saturation of the emission intensity at high current are very similar to those reported in Sec. I-A for CdSe, except that the beam current levels are considerably higher in CdS. For 40-keV electrons, the threshold was 3 mA (1.2 A/cm^2) and saturation occurred at 15 mA (6 A/cm^2). The latter effect is presumably due to heating. At 75 keV and a saturation current of about 20 mA, a peak output power of 10 W at helium temperature and 4 W at nitrogen temperature was measured, corresponding to over-all power efficiencies of 0.7 and 0.3 percent, respectively. However, since the laser emission occurred in only a few small filaments, the local efficiency is presumably much higher.

Spatial diffraction patterns from the CdS laser emission were also observed. The smallest observed pattern gave a beam angle of 4° in the direction normal to the excited surface and 6° parallel to this surface, corresponding to an emitting area 7.5 μ high and 11 μ wide. The former is consistent with the electron penetration depth, which at 50 keV is 5 to 10 μ.[13,14]

C. E. Hurwitz

C. LASER ACTION IN BULK GaAs OPTICALLY PUMPED WITH A $Ga(As_{0.94}P_{0.06})$ DIODE

In order to obtain the largest possible output power from lasers, they must be operated at maximum efficiency. One technique to produce efficient laser action is monochromatic optical pumping, where the incident energy corresponds to a pumping band of the laser material and is, preferably, only slightly larger than the energy of the lasing transition. The feasibility of monochromatic optical pumping was demonstrated by an experiment in which $CaF:U^{+3}$ was successfully pumped with an array of GaAs laser diodes.[15] This led to an attempt to produce a more efficient laser output stage by using an array of $(Ga_xIn_{1-x})As$ diodes to pump $YAG:Nd^{+3}$ (yttrium aluminum garnet doped with neodymium). However, the yield of diode lasers whose

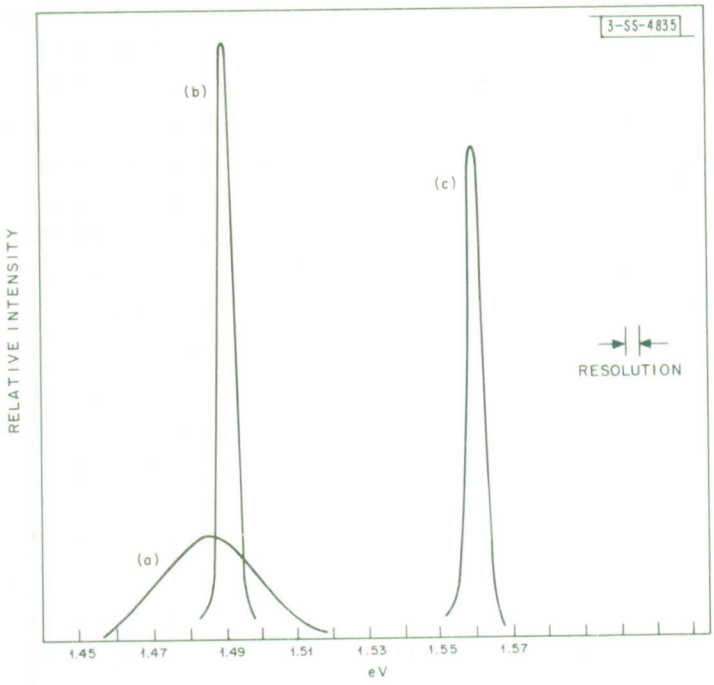

Fig. I-5. Spectral relationship between (a) bulk GaAs spontaneous emission, (b) bulk GaAs laser emission, and (c) emission from $Ga(As_{0.94}P_{0.06})$ pump laser. Amplitudes are adjusted for ease in comparison.

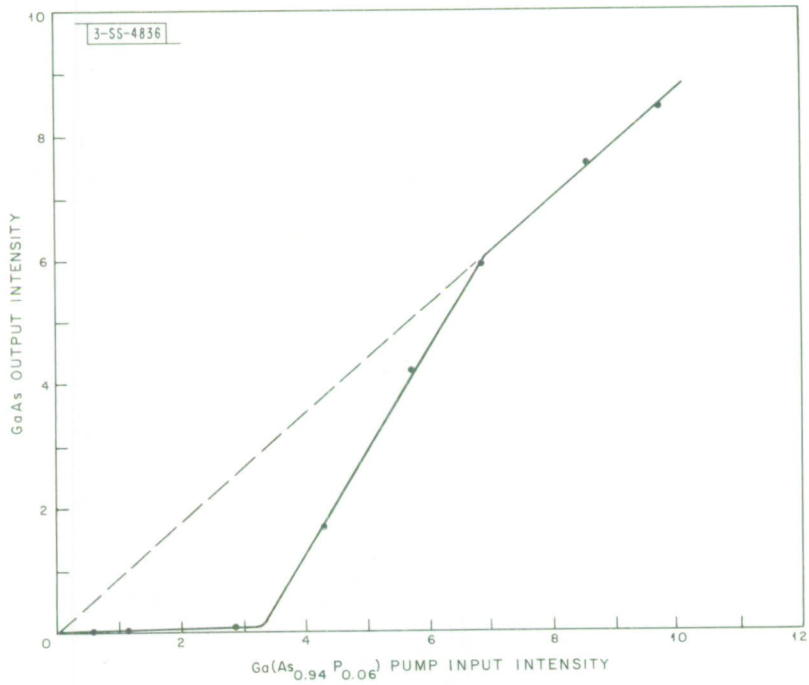

Fig. I-6. Relative GaAs emission vs $Ga(As_{0.94}P_{0.06})$ pumping emission.

emission matched the 8750 ± 50 Å pumping band of YAG:Nd^{+3} was very small and it was not feasible to fabricate arrays of these pump $(Ga_xIn_{1-x})As$ lasers.

In this section, we wish to report laser action in p-GaAs pumped with a $Ga(As_{0.94}P_{0.06})$ diode laser. Experiments by Phelan have indicated that an InSb bulk laser can be optically pumped by a GaAs diode laser with essentially 100-percent quantum efficiency.[16] On this basis, it should be possible to optically pump semiconductor lasers with a power efficiency of ν_{output}/ν_{pump}. The energy of the pump emission should be larger than the band-gap energy of the bulk semiconductor being pumped, i.e., $h\nu_{pump} > E_g$; but, while the efficiency of the output stage will be reduced slightly as the energy of the pump emission is increased above E_g, the pump energy is no longer critical, as in the pumping of the YAG:Nd^{+3}.† If, however, the energy of the pump emission can be tailored so that its absorption coefficient in the pumped bulk material is of the order of the thickness of this latter material, the population should be inverted over a "large" volume,[17] and lasing may be induced in the direction parallel to that of the pump emission.[18] In the experiment described below, the laser pump radiation impinged on the surface of a GaAs rectangular parallelepiped and the induced laser radiation was emitted perpendicular to the pump radiation.

An experimental arrangement similar to one described by Phelan[19] was used to position the sample and pump diode. The GaAs sample ($p = 4$ to 5×10^{18} cm^{-3}) and the $Ga(As_{1-x}P_x)$ pump diode were mounted on copper heat sinks in contact with liquid helium, and a cylindrical quartz lens was used to increase pump power density of the sample. Radiation emanated from a 1-mm long Fabry-Perot cavity formed by two cleaved {110} faces. In order to avoid the effects of heating, the current was applied to the pump diode in 50-nsec pulses.

The spectral relationship between the $Ga(As_{1-x}P_x)$ pump diode and the pumped GaAs is shown in Fig. I-5. The amplitudes are adjusted for ease in comparison. The measured spectral width of both the pump diode and the GaAs during lasing is due to the limited resolution of the prism spectrometer. In Fig. I-6, the intensity of the laser emission from the bulk GaAs is plotted as a function of the intensity of the emission from the pump diode. Note that above 7 on the input scale of Fig. I-6, the laser emission from the bulk is a linear function of the emission from the pump diode and the efficiency is constant. Work is now under way to measure the absolute value of this efficiency and to determine whether the output increases, as expected, when an array of pump diodes is used.

R. H. Rediker
J. H. R. Ward

D. EVIDENCE FOR IMPURITY STATES ASSOCIATED WITH HIGH ENERGY CONDUCTION BAND EXTREMA IN n-CdTe

The resistivities of several samples of n-CdTe have been found to increase by factors greater than 10^4 between 1 and 28,000 kG/cm^2 at room temperature. The interpretation of these results in terms of deionization into an impurity level‡ yields a pressure coefficient for the separation of this level from the lowest (000) conduction band large enough to suggest that the level is associated with the higher lying (100) conduction band – a model originally suggested by Paul[20] to explain Sladek's[21] results on n-GaAs.

† It should be pointed out that the pumped GaAs does not have the advantage of the longer storage time of YAG:Nd^{+3}.

‡ The word "impurity" is taken to mean any deviation from perfect periodicity in the crystal, i.e., it includes stoichiometric defects as well as chemical impurities.

Twelve samples of n-CdTe, similar to those described by Segall, Lorenz and Halsted,[22] were measured. All the samples show the same qualitative characteristic of a relative insensitivity to pressure at low pressures, followed by a sharp rise at high pressures. In Fig. I-7, we show the ρ vs P relation for five undoped samples in which a decrease in resistivity at zero pressure is believed to be correlated with an increasing excess of Cd. The samples converged to a common resistivity at high pressures. No hysteresis was observed between the curves for increasing and decreasing pressure. The other samples, which had been deliberately doped with known impurities in most cases, showed a quantitatively different resistivity dependence on temperature and pressure.

It is evident from the fact that the resistivity increases exceed 10^4 that the decrease of electron mobility caused by an increase in average electron mass, either in the (000) minimum or because of electron transfer to higher mass minima, may be ignored initially. We have therefore analyzed these results using a model with a single conduction band of state density N_c, a donor level of density N_d, and a starting electron concentration (resulting from compensation) of n_o. The donor is separated by an energy $\Delta = E_c - E_d$ from the bottom of the conduction band.

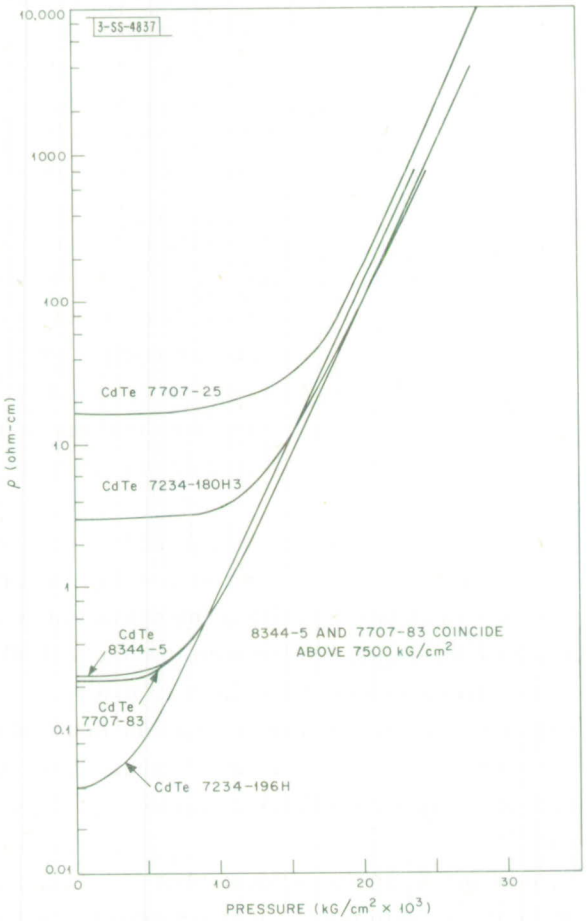

Fig. I-7. Pressure dependence of resistivity of n-CdTe.

The conduction electron density n is then given by the expression

$$n = N_c \exp[(E_f - E_c)/kT] = n_o - \frac{N_d}{1 + \alpha \exp[(E_c - E_f - \Delta)/kT]}$$

where E_f is the Fermi energy, E_c is the energy of the bottom of the conduction band, α is a degeneracy factor for the impurity, and where the approximation of Boltzmann statistics is used for the conduction band. This leads to the following expression connecting Δ and α,

$$\frac{\Delta(P)}{kT} = \ln \frac{N_c}{n_o} \cdot \frac{\alpha x(x-1)}{1 + (m-1)x}$$

where $x = \rho/\rho_o$, $\rho_o = (n_o e\mu)^{-1}$, $m = N_d/n_o$, and μ is the electron mobility in the band. At high pressures, $x \gg 1$ so that

$$\frac{\Delta(P)}{kT} = \ln \frac{N_c}{n_o} \cdot \frac{\alpha x}{m-1} \quad .$$

A graph of ln x vs P then has a slope of $[\partial\Delta(P)/\partial P]/kT$, and a zero pressure intercept of

$$\frac{\Delta(0)}{kT} - \ln \frac{\alpha}{m-1} - \ln \frac{N_c}{n_o} \quad .$$

From Fig. I-7, the five samples have identical values of $\partial\Delta(P)/\partial P$ in the region of high pressure of 12.6×10^{-6} eV/kG-cm^{-2}. The intercepts at zero pressure lead to values of $[\Delta(0)/kT] - [\ln(\alpha/m-1)]$ between 0 and -0.5.

The first and most important thing to note is that the pressure coefficient found for the ionization energy of the impurity is far greater than is expected for either hydrogenic or deep-lying impurities. In fact, the measured pressure coefficient is greater than the largest band-gap coefficient reported for CdTe.[23] Significantly, it is very close to the coefficient found for the separation with pressure of the (000) and (100) band minima in Groups IV and III-V semiconductors of the same crystal structure.[24] It seems possible, therefore, that the state of the impurity into which the conduction band is deionizing at high pressures is one described predominantly by (100) band functions.

We should like to know the absolute value of $\Delta(P)$. Unfortunately, α and m are not known, so that the zero pressure intercept $\Delta(0)$ is uncertain. Setting $\alpha = 1$ and $m = 2$ gives $\Delta(0)$ between 0 and -0.0125 eV. This does not mean, however, that the impurity level is located at this position at atmospheric pressure, since the impurity levels associated with (000) and (100) band edges may be perturbed nonlinearly as the two band edges become close in energy.

A more thorough examination of the dependence $\Delta(P)$ will require further detailed analysis of these and additional samples. We intend to examine samples with different active impurities, where we expect to find about the same value of $\partial\Delta/\partial P$, but different values of $[\Delta(0)/kT] - [\ln(\alpha/m-1)]$ and of $\Delta(P)$ near $P = 1$ kG/cm^2.

Recent pseudopotential calculations[25] place the X_1 (100) minima about 2 eV above the central Γ_1 minimum, and the L_1 minima 1.5 eV above the Γ_1 minimum. If these calculations are correct,

our interpretation of the present experiments implies a much greater contribution of the X_1 (100) band than we would intuitively expect, and it also requires an explanation of why the L_1 minima do not similarly contribute. Also, the existence of the Gunn effect oscillations[26] must be explained either on the basis that the electrons can gain the 1.5 to 2 eV of energy (note that the fundamental gap is ~1.5 eV) to reach the L_1 or the X_1 minima, or that the mobility reduction is caused by their falling into impurity levels. The resolution of these problems should give us new insight into the physics of the Gunn effect in CdTe, the striking properties of the impurities in the present experiment, and the accuracy of the pseudopotential calculations.

It is to be noted that many members of the germanium family – e.g., Ge, Sn, GaAs, InP, GaSb, GaP, and AlSb – have conduction bands with nonequivalent extrema within 0.5 eV of each other. In these cases, we suspect the appropriate description of the donor impurity states should take more account of the contributions of the higher lying extrema than has been done previously. The implications of admixture of band functions from subsidiary minima into impurity wave functions for optical properties near the fundamental gap, especially recombination phenomena, are obvious. Furthermore, the possible existence of resonant scattering states of the impurity at energy levels degenerate with the continuum provides an extra source of mobility reduction which is seldom considered.

A. G. Foyt
R. E. Halsted†
W. Paul‡

† General Electric Research and Development Center, Schenectady, New York.
‡ Harvard University, Cambridge, Massachusetts.

REFERENCES

1. C. Benoit à la Guillaume and J. M. Debever, Compt. Rend. 261, 5428 (1965), and references cited therein.
2. B. Wojtowicz-Natanson and T. Zakrzewski, Phys. Stat. Sol. 11, 873 (1965).
3. D. C. Reynolds, C. W. Litton and T. C. Collins, to be published.
4. R. B. Parsons, W. Wardzynski and A. D. Yoffe, Proc. Roy. Soc. (London) 262, 120 (1961).
5. W. Ehrenberg and D. E. N. King, Proc. Phys. Soc. (London) 81, 751 (1963).
6. C. A. Klein, Physics of Quantum Electronics, edited by P. L. Kelley, B. Lax and P. Tannenwald (McGraw-Hill, New York, 1966), pp. 424-434.
7. N. G. Basov, O. V. Bogdankevich and A. G. Devyatkov, Doklady Akad. Nauk S. S. S. R. 155, 783 (1964) [English translation: Soviet Phys. – Doklady 9, 788 (1964)]; Proceedings of the Symposium on Radiative Recombination in Semiconductors, 1964 (Dunod, Paris, 1965), p. 225; Zhur. Eksp. i Teoret. Fiz. 47, 1588 (1964) [English translation: Soviet Phys. – JETP 20, 1067 (1965)].
8. N. G. Basov, Physics of Quantum Electronics, edited by P. L. Kelley, B. Lax and P. Tannenwald (McGraw-Hill, New York, 1966), pp. 411-423.
9. C. Benoit à la Guillaume and J. M. Debever, Compt. Rend. 261, 4575 (1965).
10. D. G. Thomas and J. J. Hopfield, Phys. Rev. 128, 2135 (1962).
11. D. C. Reynolds, C. W. Litton and T. C. Collins, Phys. Stat. Sol. 9, 645 (1965).
12. D. W. Langer, Bull. Am. Phys. Soc. 6, 336 (1961), and private communication.
13. W. Ehrenberg and D. E. N. King, Proc. Phys. Soc. (London) 81, 751 (1963).
14. C. A. Klein, Physics of Quantum Electronics, edited by P. L. Kelley, B. Lax and P. Tannenwald (McGraw-Hill, New York, 1966), pp. 424-434.
15. R. J. Keyes and T. M. Quist, Appl. Phys. Letters 4, 50 (1964).
16. R. J. Phelan, Jr., private communication.
17. N. G. Basov, Physics of Quantum Electronics, edited by P. L. Kelley, B. Lax and P. Tannenwald (McGraw-Hill, New York, 1966), p. 418.
18. T. M. Quist and I. Melngailis, private communication.
19. R. J. Phelan, Jr., Physics of Quantum Electronics, edited by P. L. Kelley, B. Lax and P. Tannenwald (McGraw-Hill, New York, 1966), p. 436.
20. W. Paul, Proceedings of the International Conference on Semiconductors, Paris, 1964 (Dunod, Paris, 1964), p. 550.
21. R. J. Sladek, Proceedings of the International Conference on Semiconductors, Paris, 1964 (Dunod, Paris, 1964), p. 545.
22. B. Segall, M. R. Lorenz and R. E. Halsted, Phys. Rev. 129, 2471 (1963).
23. D. G. Thomas, J. Appl. Phys. Suppl. 32, 2298 (1961).
24. W. Paul, J. Appl. Phys. Suppl. 32, 2082 (1961).
25. M. L. Cohen and T. K. Bergstresser, Phys. Rev. 141, 789 (1966).
26. A. G. Foyt, W. Paul and A. L. McWhorter, Solid State Device Research Conference, Princeton, New Jersey, June 1965 (unpublished); A. G. Foyt and A. L. McWhorter, IEEE Trans. Electron Devices ED-13, 79 (1966).

II. OPTICAL TECHNIQUES AND DEVICES

A. GaAs – AN INTENSE, FAST, HIGH-RESOLUTION CATHODOLUMINESCENT PHOSPHOR

Measurements of the infrared radiation emitted by GaAs in the 8300- to 9000-Å spectral region when bombarded by a high-power density electron beam suggest that this compound has potential as an intense, high-speed, high-resolution phosphor. In order to calibrate this potential, some of the cathodoluminescence characteristics of GaAs are compared to those of the P-11 phosphor. Finally, the upper limit of emission intensity that can be expected from GaAs is examined.

The apparatus used to make the intensity measurements is very similar to that reported on by Cusano.[1] Beam bombardment and luminescence measurements were made at 45° with respect to the GaAs wafer, as shown in Fig. II-1. The sample (0.001 inch thick) was alloyed to a heat sink maintained at 77° or 300°K. The absolute emitted radiation intensity was measured with a calibrated 925 photodiode. Beam dimensions at the sample (0.015 × 0.020 inch) were obtained from infrared photographs of the cathode emission. Figure II-2 is a plot of the absolute emission intensity of an n-type crystal as a function of the power density of the 26-kV electron beam for heat sink temperatures of 77° and 300°K. The electron beam, maximum power capability of 6.5×10^4 W/cm^2, was pulsed on for a period of 300 nsec at a 10-Hz repetition rate. The slopes of the curves indicate that the conversion of beam power density to external GaAs radiation power density is 1.5 percent at liquid nitrogen and 0.22 percent at room temperature. The 1.5-percent efficiency at 77°K is consistent with an approximate 100-percent efficiency of conversion of hole-electron pairs into photons. Reduction of efficiency from 100 to 1.5 percent is partly due to an initial 30-percent efficiency in the conversion of beam energy into hole-electron pairs, but the greatest loss is a direct result of the small number (~4 percent) of photons that are emitted within the critical angle of the GaAs-vacuum interface.

An arrangement similar to that shown in Fig. II-1 was used to study the spatial uniformity of the GaAs emission. A fine electron beam (3-μ diameter) was scanned across the GaAs surface, and the output radiation was measured with a 7102 photomultiplier tube as a function of time. Within our experimental capability, we could not detect the variation in the emission intensity over the entire 80-beam-diameter scan. The photomultiplier noise limited our detection to variations greater than 5 percent of the signal.

Although the decay time of the GaAs emission was not measured, it is felt that its half life is very close to 10^{-9} sec as ascertained from measurements on similar crystals by storage and modulation techniques.[2]

Table II-1 lists the parameters of the GaAs phosphor and the best P-11 emitters. From many points of view, GaAs is a more perfect phosphor. It exceeds the P-11 theoretical limit by a factor of 5 in brightness, and with higher beam powers this factor can increase to 25. GaAs is faster than P-11 by a factor of 100. For high brightness, P-11 phosphor resolution is limited by grain sizes and their statistical packing distribution. For spot sizes of 20 μ, the peak-to-peak

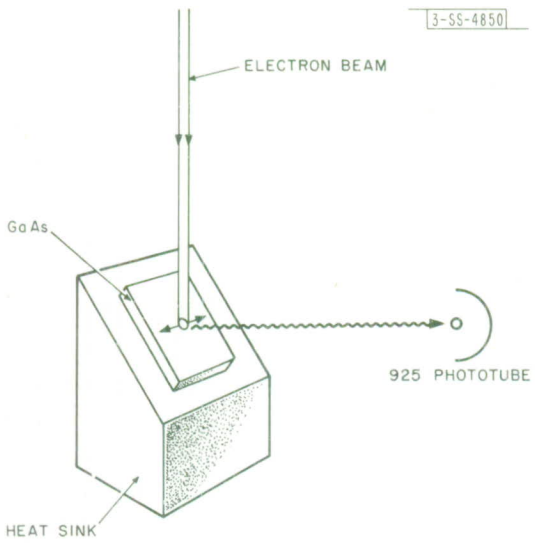

Fig. II-1. Cathodoluminescent setup used to study GaAs crystals.

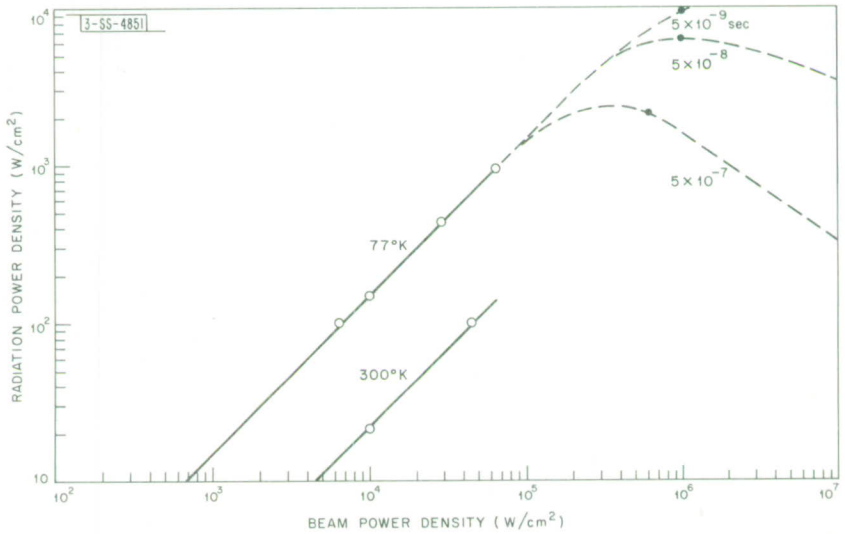

Fig. II-2. Power density emitted by GaAs as a function of electron beam power density at 77° and 300°K.

TABLE II-1

Radiator	Observed Brightness (W/cm^2)	Theoretical Maximum Brightness (W/cm^2)	Decay Time (sec)	Spatial Peak-to-Peak Fluctuations (percent)
P-11	200	200	$\sim 10^{-7}$	10
GaAs 300°K	140	~2000†	$\sim 10^{-9}$	<<5
GaAs 77°K	950	~5000†	$\sim 10^{-9}$	<<5

† Pulse duration of 5×10^{-7} sec.

fluctuations are 10 percent; for smaller beam dimensions, these fluctuations vary by almost 100 percent. Because of its single crystal structure, GaAs possesses resolutions approximating the penetration depth of the beam. The spatial fluctuations are measured to be less than 5 percent. It can be predicted with certainty that GaAs, because of its good thermal conduction, will also be more capable of sustaining high average power, when properly heat sunk, than the complex P-11 compounds. On the other hand, it should be pointed out that the P-11 phosphors are more readily made in large areas, operate efficiently at elevated temperatures, and emit in the visible portion of the spectrum.

The theoretical upper limit of cathodoluminescence brightness is obtained when the radiation levels are completely inverted, in which case

$$P_{max} = \frac{Nd}{t_s} \eta_{ex} \tag{1}$$

where N is the density of radiators, d is the electron beam penetration depth, η_{ex} is the power conversion efficiency (external radiation power/input beam power), and t_s is the spontaneous emission time. In the usual complex phosphor such as P-11, where N approaches 2×10^{18} and $t_s = 10^{-7}$, one is able to experimentally observe this saturation under short pulse bombardment. These are the emission values quoted in Table II-1. For GaAs band-to-band transitions, $N \approx 10^{21}$ while t_s has a value of 10^{-9} sec; hence, P_{max} approaches 6×10^5 W/cm^2. In practice, however, this brightness cannot be reached because the beam power required to produce the excitation raises the crystal temperature which, in turn, lowers the efficiency of the system. Using the thermal parameters of Engeler and Garfinkle[3] and an η_{ex} that varies as T^{-2}, one can estimate the maximum radiation intensity possible for a given pulse duration. These values, listed in Table II-1, can be considered as order-of-magnitude calculations which await higher electron beam power densities to lend credence to their validity.

R. J. Keyes
T. M. Quist

B. INFRARED PROPERTIES OF Mn-DOPED GaAs

The search for a material that would be suitable as a coherent heterodyne detector for the 10.6-μ CO_2 laser radiation led to a study of Mn-doped GaAs. Unfortunately, the extremely short lifetime ($\sim 10^{-13}$ sec) of the excited Mn acceptor level makes this material far more sensitive as a thermistor detector than a photoconductor of high speed.

The infrared photoresponse and the absorption coefficient of a GaAs crystal doped with 3×10^{17} Mn centers are plotted in Fig. II-3. The detector configuration is shown in the figure insert. Data were taken at a chopping frequency of 13 Hz. Subsequent pulse measurements revealed a time constant of 10^{-4} sec, which is in agreement with a calculated bolometric response time for this material in this configuration.

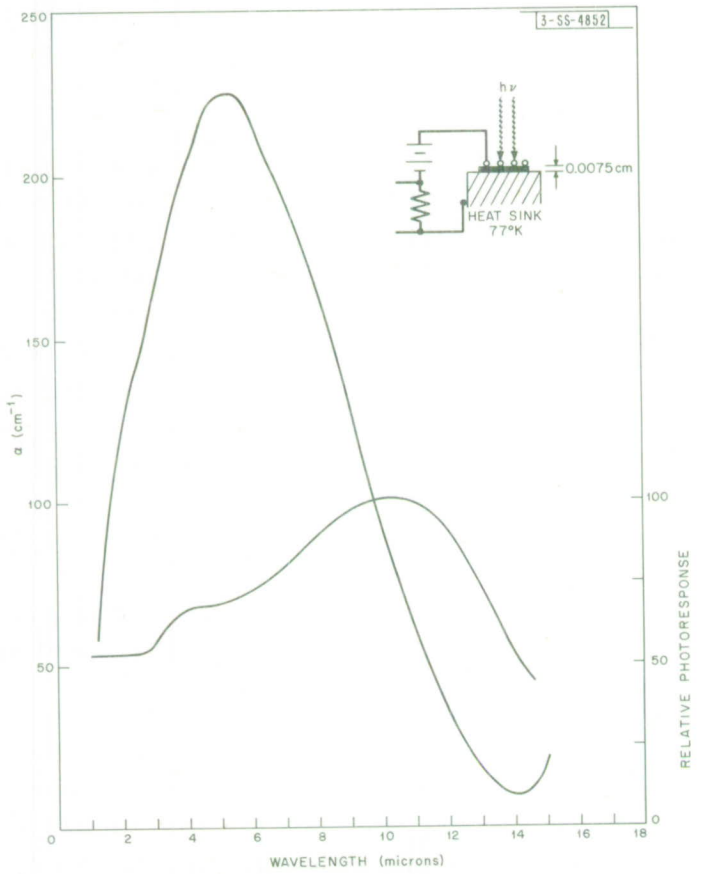

Fig. II-3. Absorption coefficient and relative photoresponse of Mn-doped GaAs at 77°K.

It should be noted that the maximum infrared absorption occurs in the region of 5 μ, and not at 12.5 μ as would be predicted from the known 0.1-eV activation energy of the Mn impurity in GaAs. Although this material has a photoconductive time constant that is too short for practical use in heterodyne detection, it has many characteristics which are ideally suited for thermistor detectors.

Jane H. Dennis
R. J. Keyes

C. PHOTOELECTRON STATISTICS PRODUCED BY A LASER OPERATING BELOW AND ABOVE THRESHOLD OF OSCILLATION

The spectrum of the light power from a laser incident upon a photomultiplier may be obtained either from spectral measurements of the anode current[4] or from photoelectron counting experiments.[5] If information on the higher order moments of the light power is desired, we must either measure the higher order spectral densities of the photomultiplier current or the higher order moments of the photoelectron count. The latter method is more convenient; in fact, we may reconstruct from the observed counts the complete probability distribution of the photoelectron emission. Probably no other experiment shows as dramatically the transition of laser operation from below to above threshold as the determination of the photoelectron statistics reported here.

The time interval within which the counts were observed was kept short (typically 10^{-6} or 10^{-5} sec) compared to the inverse bandwidth (typically 200 to 400 Hz) of the radiation emitted by the laser, except in one experiment[6] on a below-threshold laser, in which an equation recently published by Glauber[7] was verified experimentally.

We recently summarized the theory of photelectron counting and applied it to the situation in which the light incident upon the photomultiplier was narrow-band Gaussian.[6] This case leads to a Bose-Einstein[8-12] distribution for counting intervals short compared to the inverse bandwidth of the incident light. The experimentally observed slight deviation from the ideal Bose-Einstein distribution was adequately explained by assuming that the dominant mode emitted by the laser was accompanied by a small admixture of modes of broader bandwidths. A theoretical formula was developed[6] to cover this case in terms of two parameters: the total photoelectron rate, and the fraction of the power contributed by the background light. The former was directly measured, while the background could be estimated from the degree of polarization of the laser light since the dominant single axial mode was linearly polarized. As Figs. II-4(a) and (b) indicate, the theoretical curves computed this way fit the experimentally obtained points well within the spread allowed by the finite number of samples taken.

Figures II-5(a) to (c) show the data obtained with the laser operating slightly above threshold. The resulting probability distributions are close to a pure Poisson distribution

$$P(n) = \frac{\bar{n}^n}{n!}\, e^{-\bar{n}} \tag{2}$$

where $\bar{n}$ is the average photoelectron count. As before, the counting interval was short compared to the inverse bandwidth of the light, and the deviation from the Poisson distribution could be adequately explained by a small modulation of the light intensity. We may approximate this situation by assuming a Gaussian distribution law of the light intensity p around the average $\bar{p}$ giving the probability density

$$w(p) \cong \frac{1}{\sqrt{2\pi\sigma_p^2}} \exp\left\{-\frac{1}{2}\left[(p-\bar{p})/\sigma_p\right]^2\right\} \tag{3}$$

where the mean square deviation σ_p is small compared to the average light intensity $\bar{p}$. With Eq. (3) in mind, we can show that the corresponding probability distribution of photoelectrons is given by

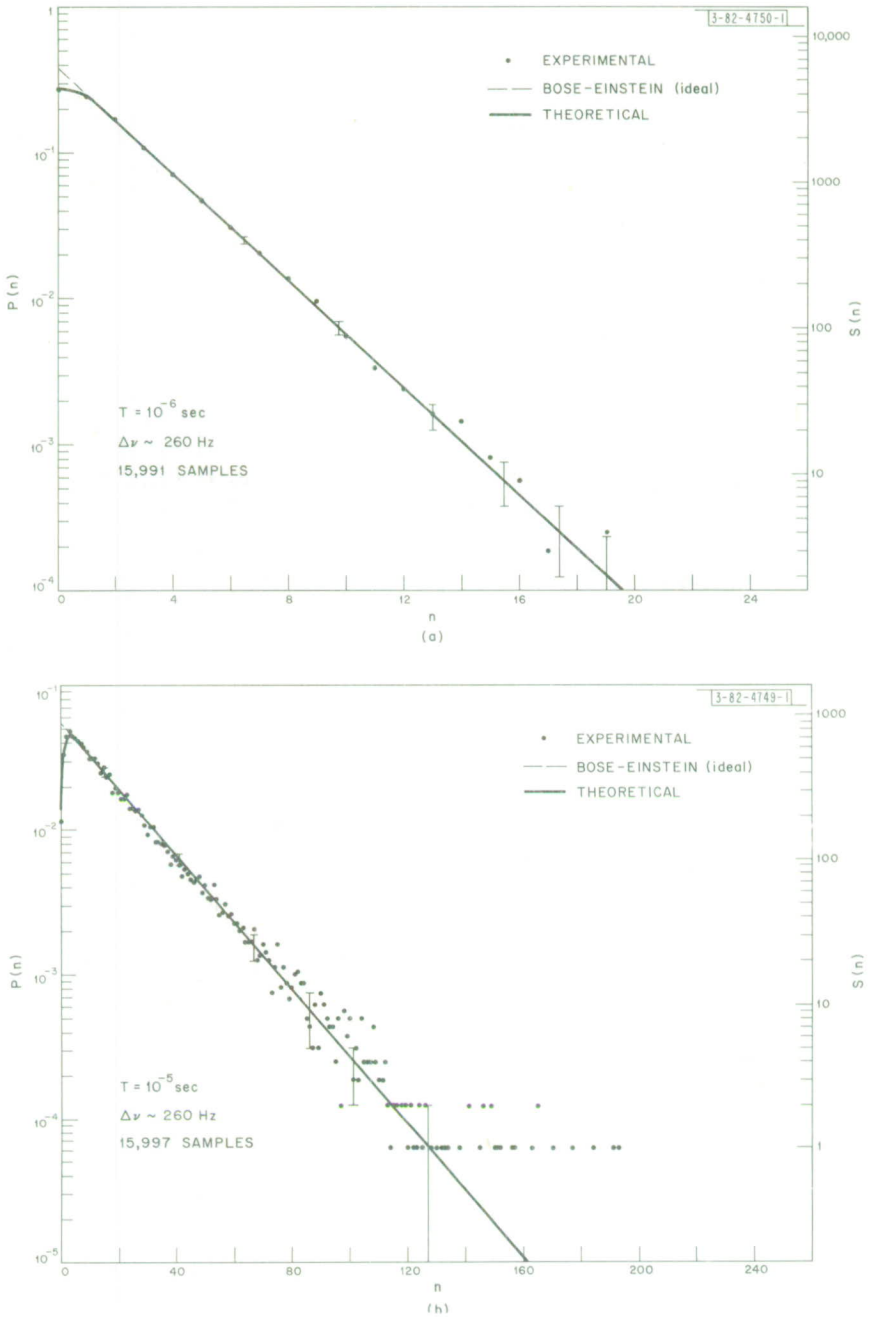

Fig. II-4(a-b). Probability distribution and number of observed samples vs photoelectron count below threshold.

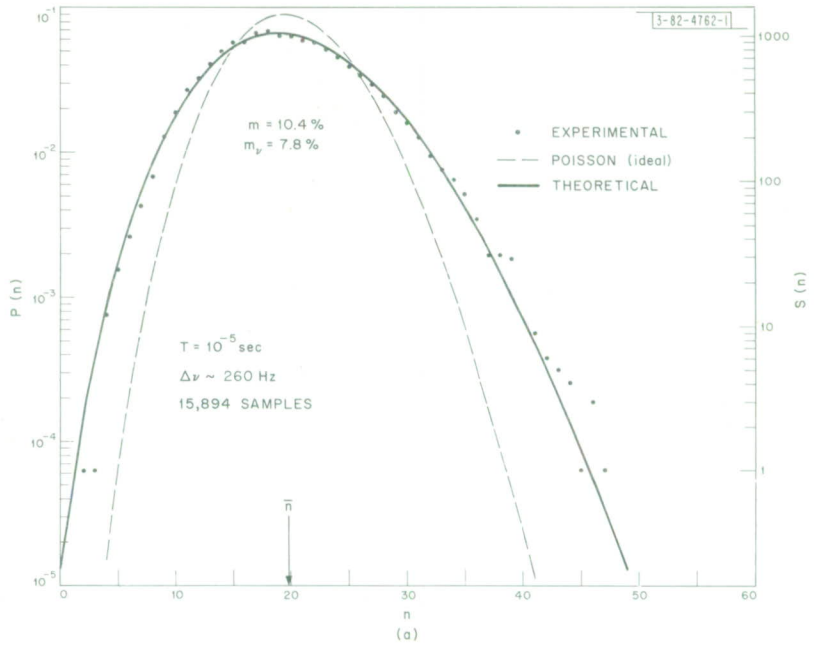

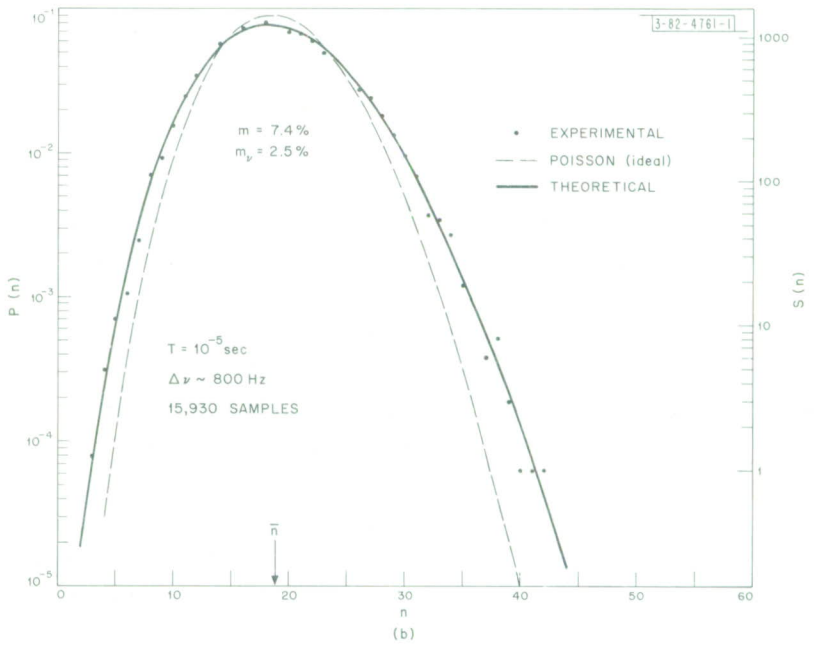

Fig. II-5(a-c). Probability distribution and number of observed samples vs photoelectron count above threshold.

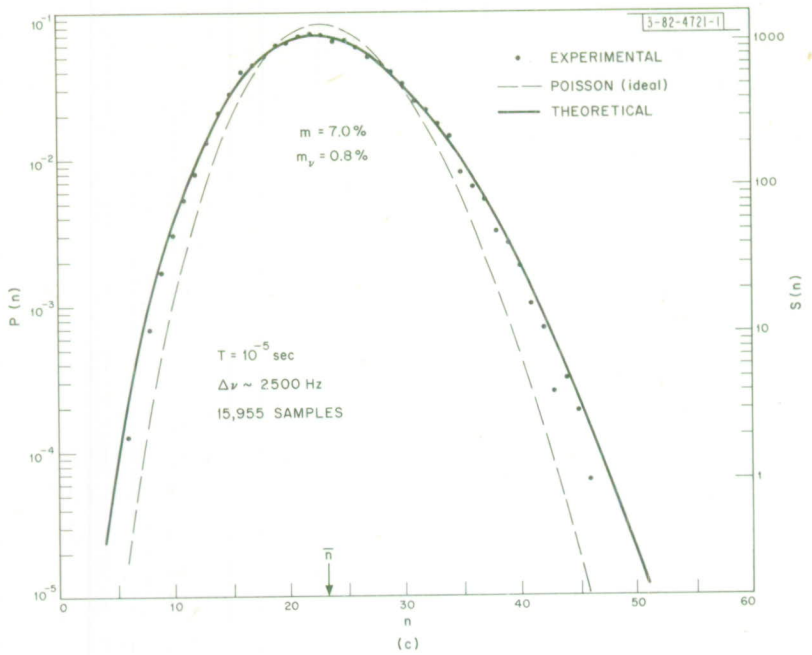

Fig. II-5. Continued.

$$P(n) = \exp\{-[\bar{n} - \sigma^2/2]\} \sum_{k=0}^{k\leq n/2} \frac{(\bar{n} - \sigma^2)^{n-2k} \sigma^{2k}}{(2^k)\,(k!)\,[(n-2k)!]} \tag{4}$$

where $\sigma^2 = \overline{n_1^2}$ is the mean square deviation (of photoelectron count), and the modulation m is defined by

$$m = \sigma/2\bar{n} \quad . \tag{5}$$

Figures II-5(a) to (c) show that the degree of modulation depended upon the power emitted by the laser, and upon external modulation. Let us assume that the modulation m on each of the figures resulted from a combination of spontaneous emission noise modulation m_ν and a residual modulation m_r which almost inevitably arose during the data-taking process because of slow random drifts and changes in quantum efficiencies, detector gains, reference voltages and resistances, temperatures, feedback effects, etc. Furthermore, it is reasonable to assume that m_r arose from random processes which were statistically independent of spontaneous noise modulation and remained constant during the few hours it took to accumulate the data for Figs. II-5(a) to (c). We have previously shown[4,5] that m_ν decreased inversely proportional to power or bandwidth near and above the threshold as expected from the van der Pol theory of oscillators. From Eq. (5), we may compute m from the measured values of σ and $\bar{n}$; from the bandwidths (measured on a spectrum analyzer), m_ν can be predicted; and from the theoretical dependence of m_ν upon the bandwidths $\Delta\nu$, m_r can be evaluated for any two of the three curves shown in Figs. II-5(a) to (c). For any pair combination, the same value of m_r = 6.95 percent was obtained.

C. Freed
H. A. Haus†

† Department of Electrical Engineering and Research Laboratory of Electronics, M.I.T.

REFERENCES

1. D.A. Cusano, Solid State Commun. 2, 353 (1964).
2. R.J. Carbone and P.R. Longaker, Appl. Phys. Letters 4, 32 (1964).
3. W. Engeler and M. Garfinkle, Solid State Electron. 8, 585 (1964).
4. C. Freed and H.A. Haus, Appl. Phys. Letters 6, 85 (1965), DDC 614737.
5. _____, Phys. Rev. 141, 287 (1966).
6. _____, Phys. Rev. Letters 15, 943 (1965).
7. R.J. Glauber, Physics of Quantum Electronics, edited by P.L. Kelley, B. Lax and P.E. Tannenwald (McGraw-Hill, New York, 1966), p. 809.
8. L. Mandel, Proc. Phys. Soc. (London) 72, 1037 (1959).
9. E. Wolf, Proceedings of the Symposium on Optical Masers, Polytechnic Institute of Brooklyn, Vol. 13 (Polytechnic Press, Brooklyn, New York, 1963), p. 29.
10. R.J. Glauber, Phys. Rev. 130, 2529 (1963).
11. _____, Phys. Rev. 131, 2766 (1963).
12. P.L. Kelley and W.H. Kleiner, Phys. Rev. 136, A316 (1964), DDC 453103.

III. MATERIALS RESEARCH

A. ANOMALY IN X-RAY SCATTERING OF ZnSe

Discrepancies between the form factors measured in x-ray diffraction experiments and the scattering functions calculated theoretically are generally attributed to uncertainties in the Hartree-Fock atomic or ionic wave functions used in the calculations. However, Kaplan and Kleiner[1] have pointed out that the usual x-ray scattering formulas ignore overlap terms. These formulas are based on a model in which the crystal wave function is approximated by a Slater determinant made up of nonorthogonal orbitals, but the charge density is calculated using the expression for orthogonal orbitals. The errors resulting from the use of this model should be especially large for metals and broad-band semiconductors, in which the electrons are quite delocalized.

In order to make a detailed comparison between theory and experiment for a broad-band semiconductor, an x-ray diffraction study has been made on ZnSe, which was selected because it has the simple zinc-blende structure and because high-purity material is available. Two different samples were used: one a commercial phosphor-grade material, and the other prepared by firing stoichiometric quantities of Zn and Se in a sealed quartz ampoule. Relative intensity measurements were made on two Norelco diffractometers employing different counting techniques. The total count for each peak was obtained in one case by step scanning at 0.01° intervals, and in the other case by scanning across the peak several times.

In calculating the relative intensities of the x-ray lines, the scaling factor s and the atomic temperature factors B_{Zn} and B_{Se} were considered as parameters, and their values were adjusted by a simplex computer program[2] to minimize the function

$$R = \sum_{hk\ell} \frac{|I_{calc}(hk\ell) - I_{obs}(hk\ell)|}{\sum_{hk\ell} I_{obs}(hk\ell)}$$

where $I_{calc}(hk\ell)$ and $I_{obs}(hk\ell)$ are the calculated and observed intensities, respectively, and $(hk\ell)$ are the Miller indices of the lines. The values of I_{calc} were obtained from the expression

$$I_{calc}(hk\ell) = s \cdot m(hk\ell) \cdot P(\Theta) \cdot |F_c|^2$$

where $m(hk\ell)$ is the multiplicity, $P(\Theta)$ is the Lorentz-polarization factor including the monochromator correction, and $|F_c|$ is the calculated structure factor (a function of B_{Zn} and B_{Se}). Two alternative calculations were made: in one case, B_{Zn} and B_{Se} were allowed to vary independently; in the other case, the restriction $B_{Zn} = B_{Se}$ = cell temperature factor was imposed. The results of these calculations are shown in Figs. III-1 and III-2, respectively. In each case, the quantity $100(I_{obs}/I_{calc})$ is plotted against $\sin\Theta/\lambda$, where Θ is the Bragg angle and λ is the x-ray wavelength.

Three groups of lines are distinguished in Figs. III-1 and III-2. One group consists of strong lines with $(hk\ell)$ all even and $(h + k + \ell) = 4n$, for which $F = f_{Zn} + f_{Se}$, where f_{Zn} and f_{Se} are atomic

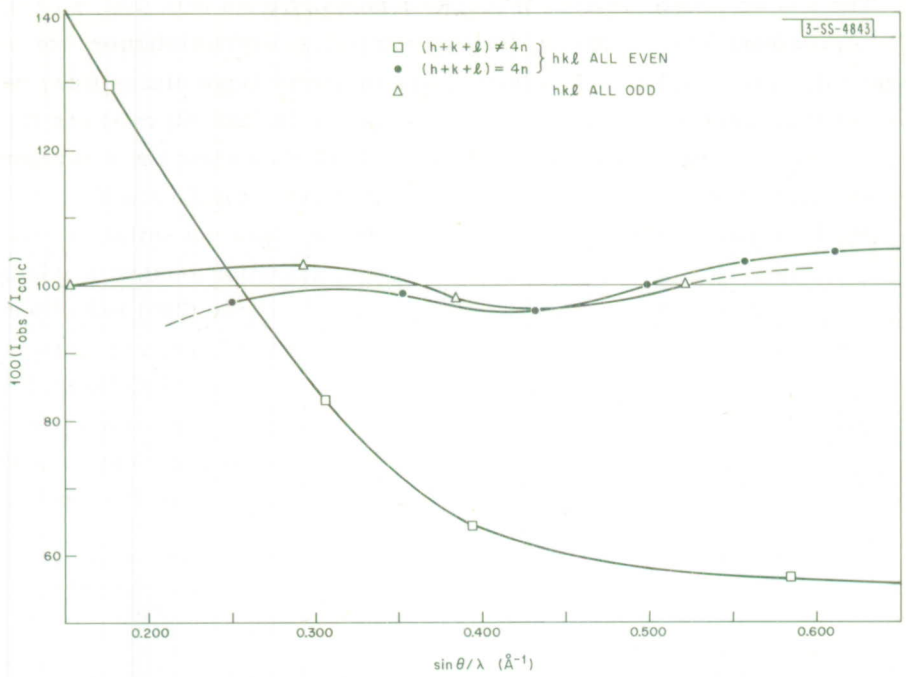

Fig. III-1. Plot of $100(I_{obs}/I_{calc})$ vs sin θ/λ for x-ray diffraction lines of ZnSe. Atomic temperature factors are $B_{Zn} = 1.34$, and $B_{Se} = 0.68$. R = 2.5 percent.

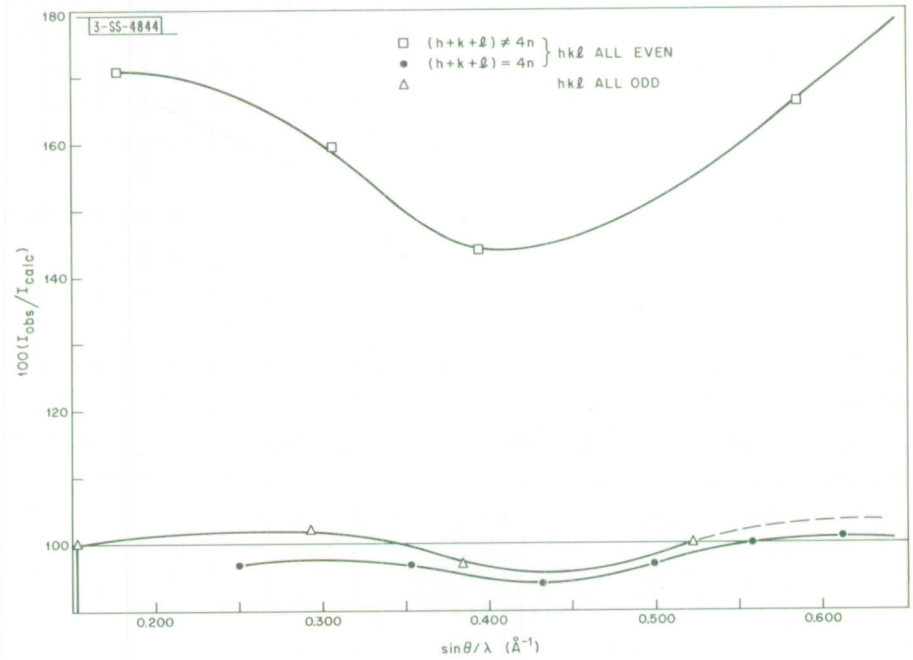

Fig. III-2. Plot of $100(I_{obs}/I_{calc})$ vs sin θ/λ for x-ray diffraction lines of ZnSe. Cell temperature factor is 0.891. R = 2.7 percent.

form factors. The second group consists of medium intensity lines with (hkℓ) all odd, for which $F = f_{Zn} \pm if_{Se}$. Agreement between theory and experiment is very satisfactory for both these groups. For the third group of lines, however, there is a very large discrepancy between the calculated and observed intensities. These are weak lines with (hkℓ) all even and $(h + k + \ell) \neq 4n$, for which $F = f_{Zn} - f_{Se}$. Comparison of Figs. III-1 and III-2 shows that the discrepancy is not reduced by introduction of individual atomic temperature factors for Zn and Se.

These results demonstrate that present scattering theory does not satisfactorily account for the observed x-ray intensities of ZnSe. A similar inconsistency for another semiconductor, GaAs, has been observed by DeMarco and Weiss,[3] who found that the (200) reflection of a single crystal was considerably larger than calculated. On the other hand, good agreement between theory and experiment is obtained for more ionic compounds, such as MgO (Refs. 4 to 6) and MnO (Ref. 7). These facts support the contention that neglect of overlap terms is an important source of error in the theoretical calculations. Experiments are being made on additional compounds to determine the relationship between the degree of covalency and the amount of discrepancy between observed and calculated intensities.

P. M. Raccah
R. J. Arnott
A. Wold*

B. ELECTRICAL PROPERTIES OF Ti_2O_3

Resistivity (ρ) and Hall coefficient (R_H) measurements at magnetic fields up to 170 kG have been carried out at the National Magnet Laboratory, M.I.T. on additional Ti_2O_3 single crystals, whose nitrogen content is between 0.07 and 0.3 atomic percent relative to Ti. The results are summarized in Table III-1.

At 4.2°K, all samples exhibit magnetoresistance ($\Delta\rho/\rho_o$) effects that are reproducible, independent of sample current, and independent of magnetic field direction. The values of $\Delta\rho/\rho_o$ increase with magnetic field strictly as H^2 for $0 < H < 170$ kG. Both ρ_o and $\Delta\rho/\rho_o$ depend on crystallographic orientation, but in a manner which differs from sample to sample. Generally, the more nearly stoichiometric and nitrogen-free the sample, the higher the values of ρ_o and of $\Delta\rho/\rho_o$ at a given magnetic field.

The R_H measurements at 4.2°K were rendered very unreliable by field-dependent misalignment voltages two orders of magnitude greater than the Hall signals. Therefore, it is only possible to give estimates for the Hall coefficients, all of which fall in the range between 1 and 40 cm^3/C.

The values of ρ_o and R_H at 77° and 273°K are appreciably lower than those at 4.2°K. Figures III-3(a-b) show the variation of $\Delta\rho/\rho_o$ and R_H at 4.2°K for Sample 5-62, whose O/Ti ratio is appreciably greater than those for the other samples in this series. Deviations from the linear dependence of $\Delta\rho/\rho_o$ on H^2 and variations of R_H with H are observed; however, the values of ρ_o and R_H at 77°K are comparable with those of the other samples.

---

* Division of Engineering, Brown University.

TABLE III-1
ELECTRICAL PROPERTIES OF Ti_2O_3

Sample	Sample Orientation (angle of current direction with c-axis) (deg)	4.2°K		77°K	
		ρ (ohm-cm)	Slope × 10^3 of Plot of $\Delta\rho/\rho_o$ vs H^2	ρ (ohm-cm)	cm^3/C
6368	22.5	2300	0.067	0.20	0.43
	45	630	0.086	0.11	0.22
	90	130	0.071		0.22
6365	22.5	79	0.074	0.059	0.12
	45	72	0.075	0.068	0.12
	90	42	0.074	0.050	0.11
6970	0	17	0.059	0.049	0.085
	22.5	26	0.062	0.11	0.070
	45	21	0.068	0.081	0.088
	67.5	21	0.059	0.061	0.069
	90	37	0.071	0.053	0.097
6970 (Sc-doped)	0	8.7	0.063	0.061	0.12
	22.5	3.2	0.068	0.024	0.15
	45	4.6	0.071	0.027	0.16
	67.5	5.2	0.070	0.034	0.19
	90	6.5	0.072	0.033	0.17
5-62	90	0.054	0.044*	0.050	0.037

* Initial slope; plot became nonlinear for H > 60 kG.

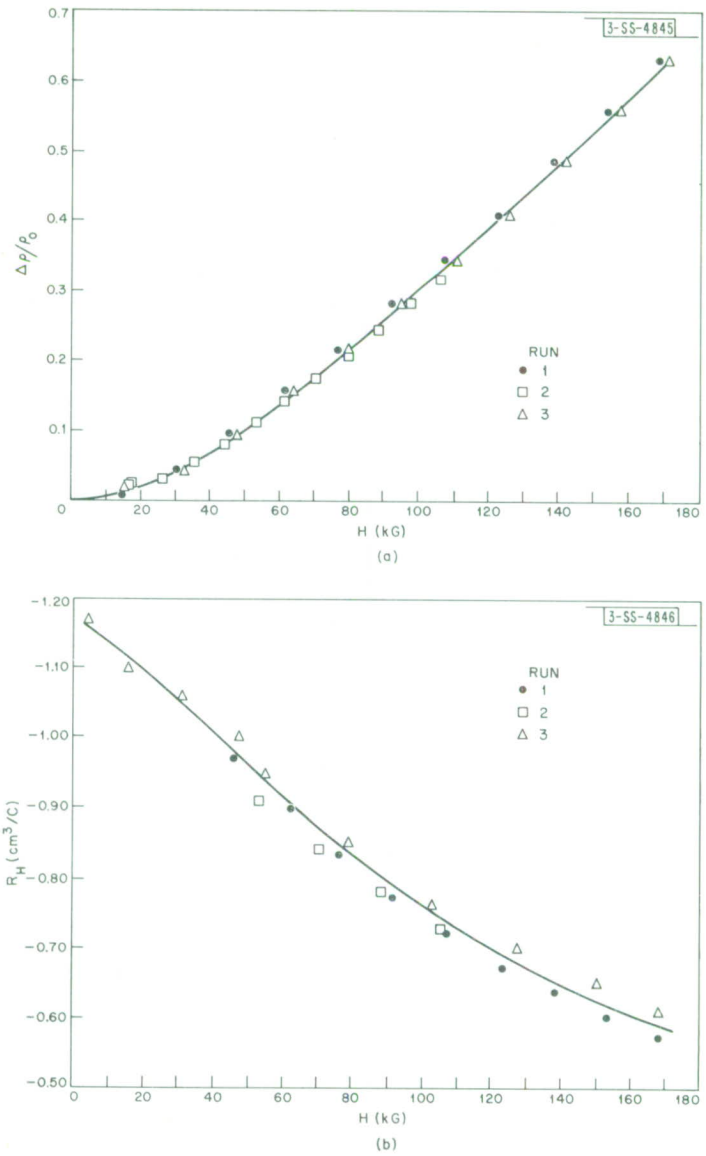

Fig. III-3. Electrical properties of Ti_2O_3 Sample 5-62 at 4.2°K as a function of magnetic field. Current direction perpendicular to c-axis. (a) Magnetoresistance; (b) Hall coefficient.

The new data are consistent with our previously proposed model, according to which mixed conduction occurs in Ti_2O_3 at 4.2°K, whereas hole conduction takes place at 77° and 273°K.

J. M. Honig
R. E. Fahey
J. T. Roddy

C. LASER MATERIAL STUDIES

During earlier experiments on the cathodoluminescence and thermoluminescence from a variety of materials, including CaF_2:Y (Ref. 8) and CaF_2:Mn, intense luminescence was observed from Al_2O_3:Cr (ruby) excited by a pulsed beam of ~1 MeV electrons. However, this luminescence was found to saturate and then decrease as the beam current was increased. In order to find an explanation for this effect, optical absorption and EPR measurements have been made on electron-irradiated ruby. Preliminary results indicate that under irradiation the reaction $2Cr^{+3} \rightleftharpoons Cr^{+2} + Cr^{+4}$ is forced to the right. This could account for the observed decrease in luminescence, since neither Cr^{+2} nor Cr^{+4} fluoresces and, furthermore, Cr^{+4} appears to quench the fluorescence of Cr^{+3}. The data also indicate that $Cr^{+3}(3d^3)$ acts as a trap for both electrons and holes.

In other experiments, (1) stimulated emission from Nd^{+3} in YVO_4, a new laser host, was obtained at a pulsed threshold of about 200 J from a crystal grown by the Linde Corporation; (2) direct evidence has been obtained for energy exchange between the lattice and Nd^{+3} ions in CeF_3:Nd; and (3) laser action has been observed in ruby grown from the vapor at about 1700°C by Lexington Laboratories, Inc.

J. R. O'Connor

D. OUTER ELECTRONS IN α-IRON

Relevant data on the eight outer electrons of α-iron are summarized in Table III-2. The outer-electron configuration consistent with these data is

$$t_{\uparrow}^{3-0.7\gamma}\, t_{\downarrow}^{2.06-0.7\gamma}\, e_{\uparrow}^{1.61-0.3\gamma}\, e_{\downarrow}^{0.55-0.3\gamma}\, c_{\uparrow}^{0.41+\gamma}\, c_{\downarrow}^{0.37+\gamma}$$

where $0 \leqslant \gamma \lesssim 1$ is a measure of the uncertainty in the number of 4s and 4p broad-band conduction electrons c. The subscripts refer to spin states; the superscripts refer to numbers of electrons per atom. The 3d orbitals of t symmetry are directed toward nearest neighbors, those of e symmetry toward next-nearest neighbors. A significant feature of this configuration is the fact that there is only a partial spontaneous magnetization of the 3d bands.

A single band in a two-sublattice structure would have the following low-temperature magnetic order as a function of the fraction of band states that are occupied: (1) $0 \leqslant f \leqslant f_1$, no long-range order; (2) $f_1 < f \leqslant f_2$ where $f_2 \lesssim \frac{1}{4}$, ferromagnetism or superconductivity; (3) $f_2 < f < \frac{1}{2}$, spin-density wave with decreasing wavelength as $f \rightarrow \frac{1}{2}$; (4) $f = \frac{1}{2}$, antiferromagnetic spin-density wave; (5) $\frac{1}{2} < f < \frac{3}{4}$, spontaneous ferromagnetic component with spin contribution to atomic moment $\approx (f - \frac{1}{2})\,\mu_B$, which is analogous to ferromagnetic component of localized electrons coupled antiparallel by superexchange, but canted by double-exchange coupling to mobile electrons; and, finally, (6) $\frac{3}{4} \leqslant f < 1$, conventional band ferromagnetism with decreasing Curie temperature and atomic moment $(1 - f)\,\mu_B$ as $f \rightarrow 1$. Partial spontaneous magnetization of the 3d bands of α-iron is consistent with the fact that $f = 0.722 - 0.2\gamma$, or $\frac{1}{2} < f < \frac{3}{4}$.

TABLE III-2
DATA ON 3d ELECTRONS OF α-IRON

Property	Measured Value	Reference
Electron density symmetry[a]	(0.70 ± 0.02) t, (0.30 ∓ 0.02) e	9
Spin-density symmetry[b,c]	(0.47 ± 0.01) t, (0.53 ∓ 0.01) e	10,11
M_s (0°K)	2.218 μ_B/atom	12
Spectroscopic g	2.17	12
Number outer 3d electrons	6 ± 1.5	13

a. Spherical form factor corresponds to 0.6t, 0.4e. Orbitals of t symmetry are directed toward nearest neighbors, those of e symmetry toward next-nearest neighbors.

b. Experimental and theoretical form factors can be reconciled by introducing a uniform negative magnetization of $-0.21\ \mu_B$/atom. This implies a net positive 3d magnetization of $(2.22+0.21)\ \mu_B = 2.43\ \mu_B$ at room temperature.

c. At largest distances from atomic nuclei, net spin density is negative. Along next-nearest-neighbor join, net spin density is everywhere positive; along nearest-neighbor join, it is small, and may be negative, at the midpoint. Thus, zones of negative spin density are toroidal with centers at midpoints of next-nearest-neighbor joins and toroidal planes perpendicular to these joins. Toroidal zones intersect in regions of space most distant from any atomic position.

With the aid of magnetic and electronic-specific-heat data for the systems $Cr_{1-x}Mn_x$, $Fe_{1-x}Mn_x$, and $Fe_{1-x}Co_x$, it is possible to argue that the number of broad-band electrons in Cr, Mn, and Fe are $n_c^{Cr} = 3.0$, $n_c^{Mn} \approx 2.0$, and $n_c^{Fe} \approx 1.0$ (or $\gamma = 0.11$). This leads to Figs. III-4 to III-6, which illustrate the schematic density-of-states vs energy curves for the 3d electrons of Cr, CrMn, and α-iron.

Finally, the larger intra-atomic-exchange contraction for electrons of positive spin relative to those of negative spin can account qualitatively for the spin-density distributions reported in footnotes b and c of Table III-2. It does not appear necessary to postulate a negative s-d coupling.

J. B. Goodenough

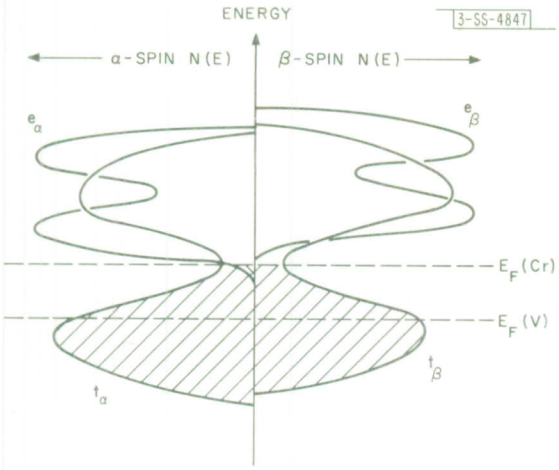

Fig. III-4. Schematic one-electron density-of-states N(E) vs energy for 3d bands of Cr, given the electron configuration d^3c^3. Numbers refer to numbers of electrons per atom represented by area under the corresponding maxima in the curves.

Fig. III-5. Schematic one-electron density-of-states N(E) vs energy for 3d bands of one simple-cubic sublattice of disordered CrMn. Ferromagnetic next-nearest-neighbor interactions, antiferromagnetic nearest-neighbor interactions. Corresponding diagram for other simple-cubic sublattice has a reversal of α- and β-spins.

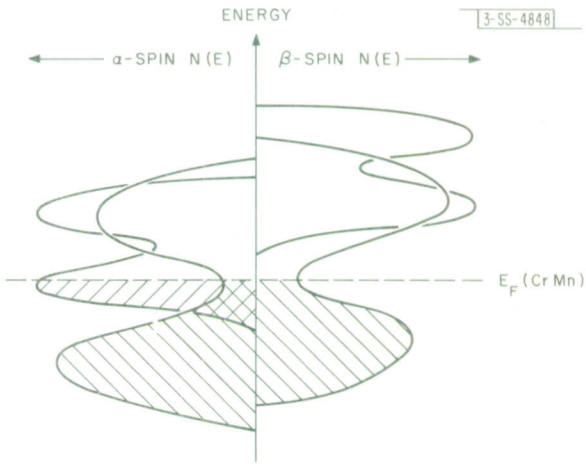

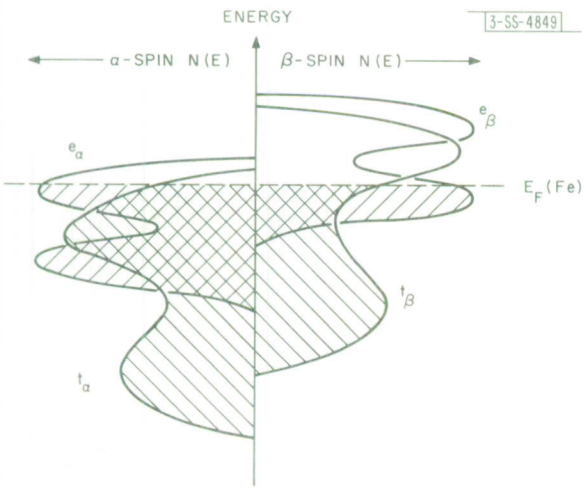

Fig. III-6. Schematic one-electron density-of-states N(E) vs energy for 3d bands of α-iron. Ferromagnetic nearest-neighbor and next-nearest-neighbor interactions.

REFERENCES

1. T.A. Kaplan and W. Kleiner, private communication.
2. Solid State Research Report, Lincoln Laboratory, M.I.T. (1965:2), p.33, DDC 624611, H-686.
3. J.J. DeMarco and R.J. Weiss, Phys. Letters (Amsterdam) 13, 209 (1964).
4. G. Burley, J. Phys. Chem. Solids 26, 1605 (1965).
5. S. Togawa, J. Phys. Soc. Japan 20, 742 (1965).
6. P.M. Raccah and R.J. Arnott (to be published).
7. M. Kuriyama and S. Hosoya, J. Phys. Soc. Japan 18, 1315 (1963).
8. J.R. O'Connor, Appl. Phys. Letters 4, 126 (1964).
9. J.J. DeMarco and R.J. Weiss, Phys. Letters (Amsterdam) 18, 92 (1965).
10. C.G. Shull and Y. Yamada, J. Phys. Soc. Japan 17, Supp. B-III, 1 (1962).
11. C.G. Shull and H.A. Mook, Phys. Rev. Letters 16, 184 (1966).
12. R.M. Bozorth, Ferromagnetism (Van Nostrand, New York, 1951).
13. B.W. Batterman, D.R. Chipman and J.J. DeMarco, Phys. Rev. 122, 68 (1961).

IV. PHYSICS OF SOLIDS

A. ELECTRONIC BAND STRUCTURE

1. Optical Constants of ReO_3

Analysis of the room-temperature reflectivity measurements[1] of ReO_3 single crystals is continuing. The low-energy reflectivity data were found to be well fitted by a Drude free electron equation for the complex dielectric constant of the form

$$\epsilon^f = 1 - \frac{\omega_{p_a}^2}{\omega(\omega + i\gamma)} + C \qquad (1)$$

where C is a contribution from bound electrons, ω_{p_a} is the plasma frequency, and γ is the scattering frequency. The Drude curve was determined by a least squares fit to the data below 2.2 eV. The parameters thus obtained are $\omega_{p_a} = 5.5$ eV, and $1/\gamma = \tau_c = 2.03 \times 10^{-14}$ sec.

Assuming one free electron per rhenium atom, we calculated an effective mass of 0.87 m_o and a conductivity of 1.31×10^5 ohm^{-1} cm^{-1}, which is in good agreement with the measured DC conductivity of 1.47×10^5 ohm^{-1} cm^{-1}.

Two different Kramers-Kronig methods were programmed on the IBM 7094 computer to obtain the optical constants. These separate results give an estimate of the sensitivity of the computed constants to the approximations made for the reflectivity beyond 12 eV as required by the Kramers-Kronig integrals. The agreement of the methods over the 12-eV range is better than 20 percent in absolute magnitude. Of more significance, the peak positions and shapes of the optical constant curves are nearly identical.

Figure IV-1 shows the energy dependence of the index of refraction n and the extinction coefficient k. Below 2.3 eV, n and k have the typical behavior of a free electron plasma in metals. The fact that k reaches a small value before the onset of any interband effects is a necessary condition for the reflectivity plasma edge to reach a value of less than 2 percent at the 2.3-eV minimum. This is the energy at which the metal becomes transparent to radiation and, indeed, an examination of thin deposits of ReO_3 reveals they are green in transmitted light while the crystals are red in reflected light.

The real and imaginary parts of the dielectric constant $\epsilon = \epsilon_1 + i\epsilon_2$ obtained by the Kramers-Kronig analysis of the data are displayed in Fig. IV-2. A further breakdown of ϵ_1 into free and bound electron contributions was found by a Kramers-Kronig analysis of ϵ_2 using the method described by Ehrenreich and Philipp.[2] These resulting curves are also shown in Fig. IV-2. It is seen that the first interband transition occurs at 3.8 eV and is well separated from the plasma energy at 2.17 eV. Other strong interband transitions occur at 6.9 and 9.2 eV. The effective number of absorbing electrons, which is related to the oscillator strengths up to the frequency ω_o, is obtained from the relation

$$n_{eff} = \frac{2\pi^2 e^2 N}{m_o} \int_o^{\omega_o} \omega \epsilon_2(\omega)\, d\omega \qquad (2)$$

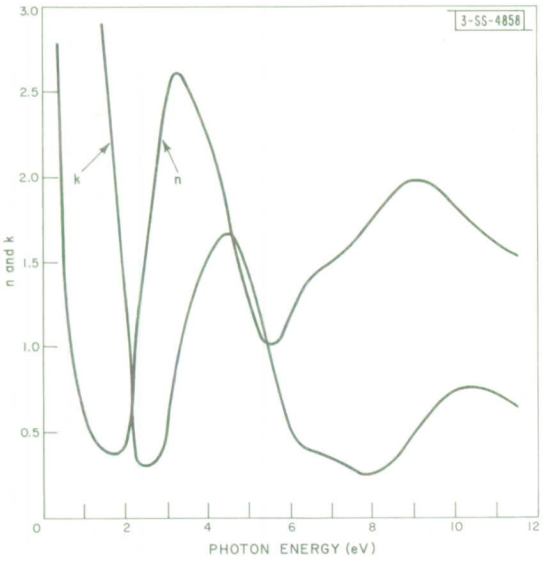

Fig. IV-1. Variation, with photon energy, of index of refraction n and extinction coefficient k of ReO_3 at room temperature.

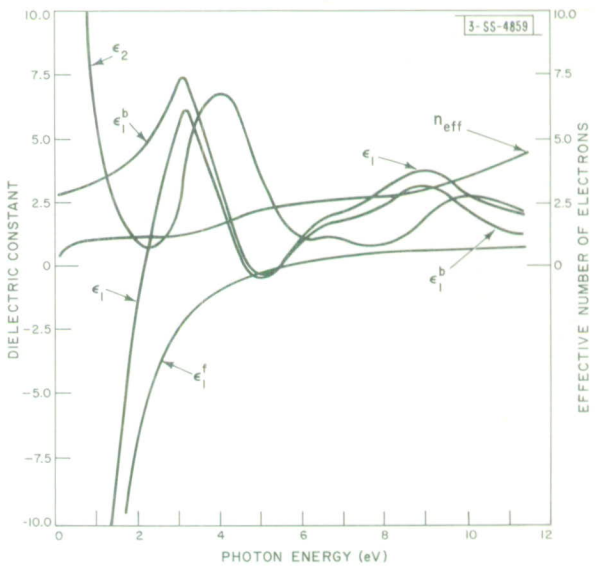

Fig. IV-2. Real and imaginary parts of dielectric constant ϵ_1 and ϵ_2, respectively, of ReO_3. ϵ_1 is resolved into free and bound contributions ϵ_1^f and ϵ_1^b, respectively. n_{eff} is effective number of electrons as obtained from ϵ_2.

where N is the density of atoms. Equation (2) is plotted in Fig. IV-2. Below the onset of the interband transitions, $n_{eff} \approx 1.1$ which is the reciprocal of the optical effective mass ratio of the conduction electrons. The first interband transition increases n_{eff} to about 2. This increase by one electron may be consistent with a transition from the Fermi level to an empty conduction band.

A plot is given in Fig. IV-3 for the loss function

$$\frac{\epsilon_2}{\epsilon_1^2 + \epsilon_2^2} \quad . \tag{3}$$

The first peak corresponds to the "hybrid" plasma resonance at the observed plasma frequency. The peak at 5.7 eV is connected with the "free" electron plasma, though slightly modified by screening effects.

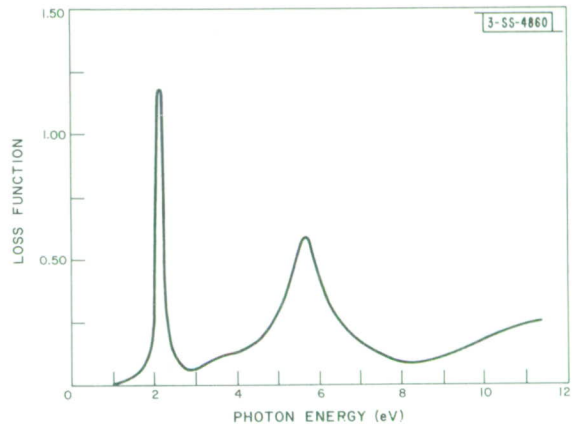

Fig. IV-3. Loss function vs photon energy.

These data are now being compared with theoretical band calculations, and will be extended to higher energies in continuing investigations.

J. Feinleib
W. J. Scouler

2. Magnetoabsorption of Direct Transition in GaSe in Voigt Geometry and at 1.5 °K†

Work on the high field oscillatory magnetoabsorption of the direct transition in the layer compound GaSe is being continued and extended. The spectra observed in the Voigt configuration have been determined to be isotropic with respect to the direction of H in the c-plane, the radiation being propagated along the c-axis. In terms of the band structure, this would imply that band edges at positions other than at the center of the zone are unlikely.[3] For linearly polarized radiation, essentially the same spectra are obtained for E || H and E ⊥ H. The n = 2 exciton state associated with the lowest Landau level exhibits appreciable splitting (4.8 meV at 85 kG), as shown in Fig. IV-4 (in the vicinity of the wavelength drum reading 1280); however, no such splitting is

† This experiment was carried out using the high field facilities of the National Magnet Laboratory, M.I.T.

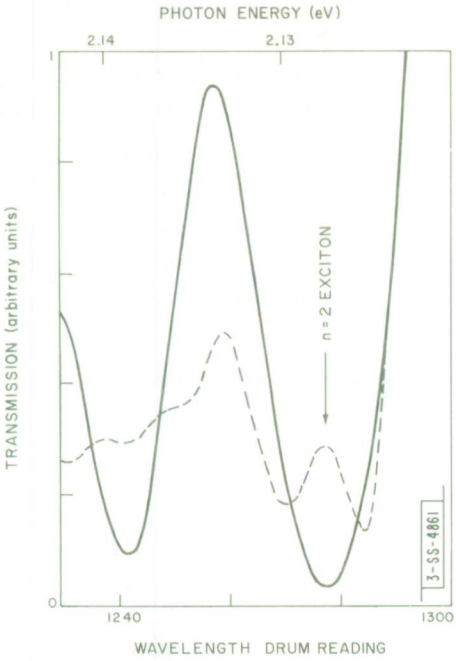

Fig. IV-4. Splitting of n = 2 exciton state associated with lowest Landau level in Voigt configuration (dashed line); Faraday configuration (solid line) magnetoabsorption spectrum exhibits no such splitting.

observed in the Faraday configuration. This behavior can be explained on the basis of an anisotropic g-factor that depends on the angle which the magnetic field makes with the c-axis.

J. Halpern

3. Optical Absorption in Crossed Electric and Magnetic Fields in GaSe†

As a possible method of obtaining separately the parameters of the valence and conduction bands of GaSe and thus further elucidating the band structure, we have initiated a program to study the optical absorption of this material in crossed electric and magnetic fields. In the experiments described in Sec. IV-A-2 and in a previous Solid State Research Report,[3] only the reduced masses and g-factors are obtained; here, with the addition of an electric field we expect to break down some of the selection rules which hold for the direct transition.

Preliminary experiments have been carried out both at room temperature and at 1.5 °K using magnetic fields up to 86 kG (with H || propagation vector || c-axis) and 3-kHz sinusoidal electric fields up to 800 V cm^{-1} peak-to-peak. Differential spectra were observed at 6 kHz, both in the vicinity of the band edge and in the region of the "quasi-Landau levels." Comparison of these results with the theoretical calculations of Vrehen[4] indicates that these initial samples exhibited an $\omega_c\tau \sim 3$, which is just below the threshold at which one would expect to see additional structure over that observed in simple magnetoabsorption.

We also observed that the application of small DC electric fields greatly reduces the peaks in the oscillatory magnetoabsorption.

J. Halpern

† This experiment was carried out using the high field facilities of the National Magnet Laboratory, M.I.T.

4. Electroluminescence in GaSe†

During the crossed field work (see Sec. IV-A-3), we observed that the application of electric fields to some of the GaSe samples gave rise to electroluminescence. This phenomenon has recently been reported at 77 °K by Akhundov.[5,6] The luminescence appeared in parallel filaments around the periphery of the sample as shown in Fig. IV-5; it was excited by an AC field of ~ 600 V cm^{-1} peak-to-peak at 1.5 °K. Two emission peaks at 1.968 and 1.948 eV, of 10- and 15-meV widths, respectively, were measured in addition to a rather broad (~ 35 meV) peak at ~ 1.92 eV; the latter is probably the same peak observed in Ref. 6. The emission spectrum cuts off sharply on the high-energy side at 1.986 eV. Unfortunately, this particular sample deteriorated before measurements could be made on the low-energy end of the spectrum; other luminescent samples will be examined subsequently.

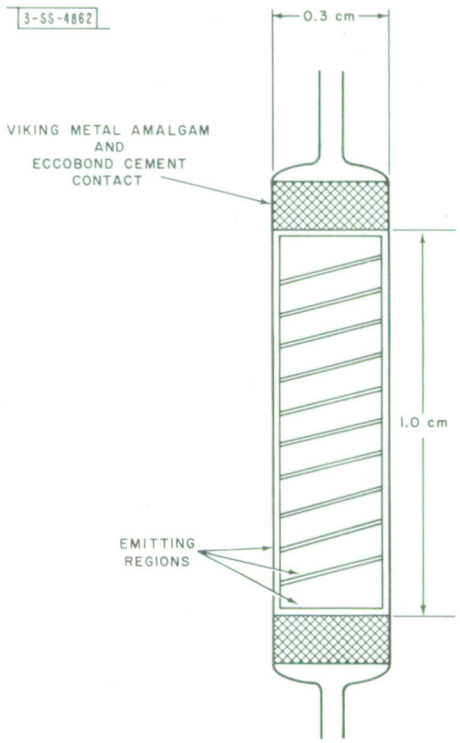

Fig. IV-5. Appearance of emitting regions of GaSe sample No. 659 at 1.5°K when excited by an AC electric field of ~ 600 V cm^{-1} peak-to-peak.

We also qualitatively observed that the introduction of a magnetic field strongly reduced the luminescence: a field of ~ 25 kG decreased the emitted intensity by approximately a factor of two; further increases of magnetic field (up to 86 kG) diminished the intensity by approximately an additional factor of two.

J. Halpern

5. Interband Magnetoreflection in HgTe†

Two sets of magnetoreflection oscillations have been observed in HgTe near 4 °K at fields up to 100 kG. One set, summarized in Fig. IV-6, was observed between photon energies of 0.05

† This experiment was carried out using the high field facilities of the National Magnet Laboratory, M.I.T.

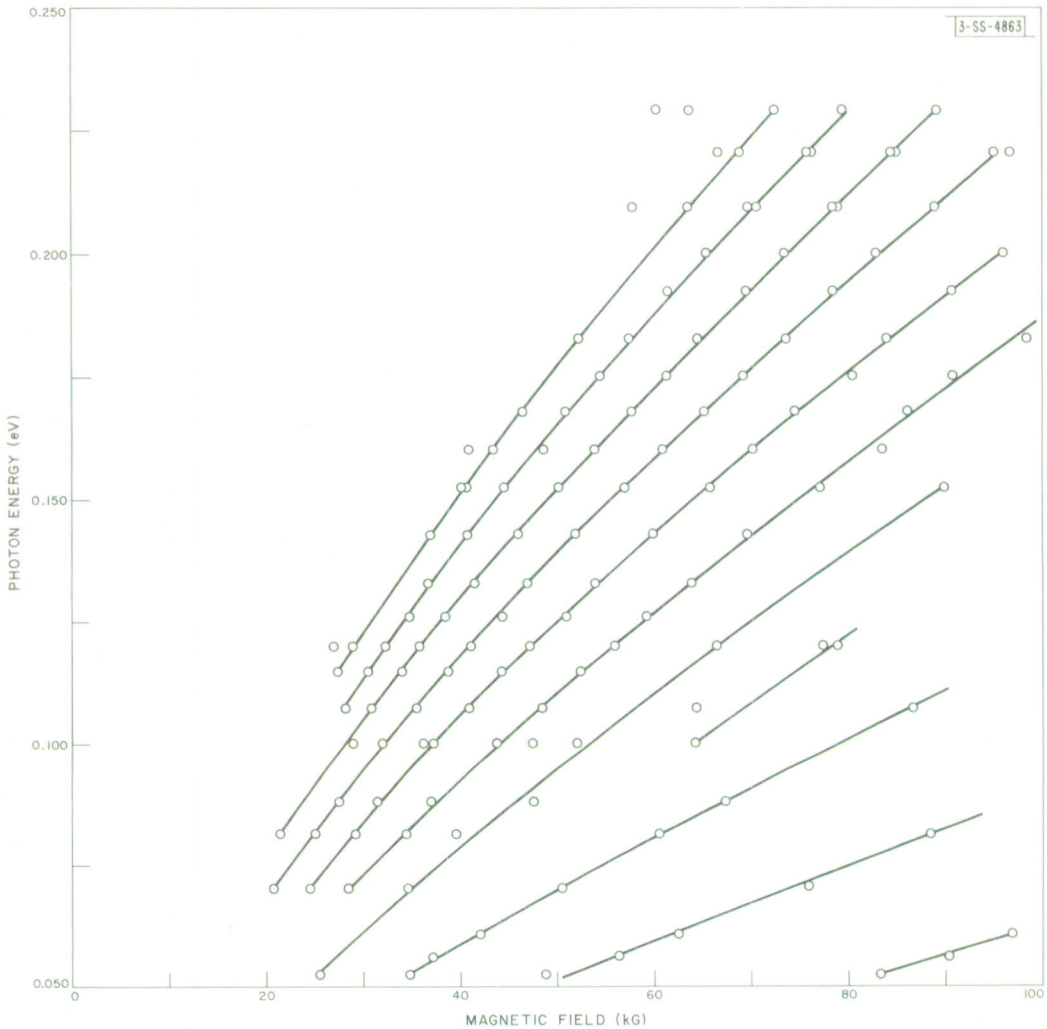

Fig. IV-6. Low-energy transitions for HgTe.

to 0.23 eV and an extrapolation of the data to H = 0 yields an energy gap of, or near, zero. The other set, presented in Fig. IV-7, was found between 0.30 and 0.38 eV and extrapolates at zero field to an energy gap between 0.285 and 0.290 eV.

Figure IV-8 shows an inverted or gray tin-like band structure which is used to interpret these magnetoreflection oscillations. The valence band maximum and conduction band minimum are degenerate at k = 0 and have Γ_8 symmetry. The low-energy oscillations arise from transitions across this zero energy gap which are indicated by arrow A in Fig. IV-8. The next valence band also has its maximum at k = 0 and has Γ_6 symmetry. Transitions between this band and the conduction band, indicated by arrow B in Fig. IV-8, give the higher energy oscillations. The zero field extrapolation of the lines in Fig. IV-7 gives $E(\Gamma_8) - E(\Gamma_6)$.

The lines in Figs. IV-6 and IV-7 are not theoretical curves but simply guides for following the field dependence of the transitions. A comparison with theory is now being carried out with a method which was devised by Pidgeon and Brown[7] for a detailed interpretation of interband magnetoabsorption in InSb. This combines the methods of Luttinger and Kohn, and Bowers and Yafet and treats the mutual interaction between the Γ_6, Γ_7, and Γ_8 bands exactly and their interactions with higher bands to order k^2.

The energy, $E(\Gamma_8) - E(\Gamma_6)$, and the momentum matrix element between these states largely determine the curvature of the Γ_8 conduction band because other interacting bands are remote.

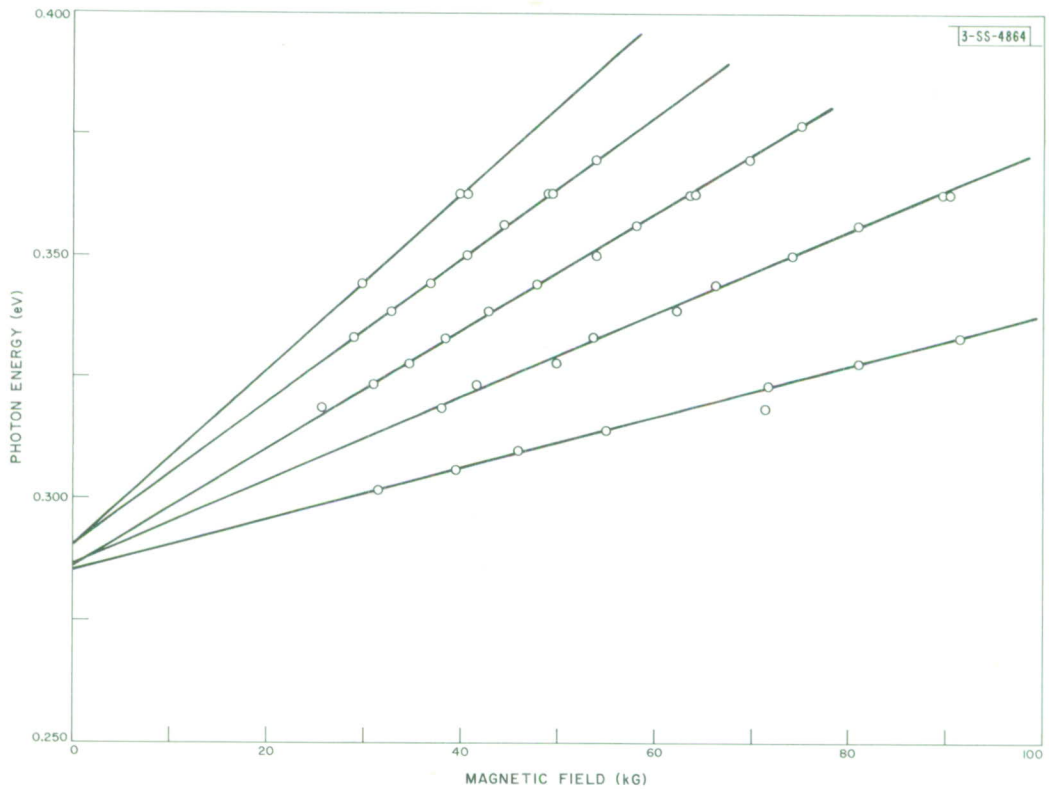

Fig. IV-7. High-energy transitions for HgTe.

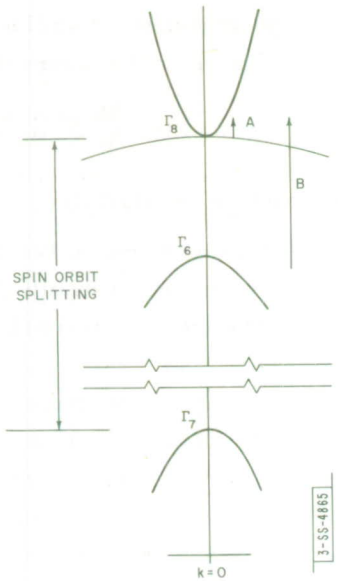

Fig. IV-8. Band structure of HgTe.

Previous intraband optical and magneto-optical determinations of the conduction band effective mass vs electron concentration, made at room temperature, suggest that $E(\Gamma_8) - E(\Gamma_6) = 0.15$ eV, about half the value reported here for this gap near 0 °K. When the theoretical fitting of the transitions is complete, it should be possible also to compare the size of the momentum matrix element as given by the two methods. At present, the factor of two disagreement in $E(\Gamma_8) - E(\Gamma_6)$ has not been explained.

Finally, the observation of these two sets of transitions is additional evidence for the applicability of the gray tin band structure to HgTe. At this stage of interpretation, nothing has been said about the unsettled question of whether or not the Γ_8 valence band in some directions first goes upward and then downward in energy as k increases from zero, giving a negative rather than zero thermal energy gap.

S. H. Groves
R. N. Brown†

6. Magnetoreflection in Bi‡

Magnetoreflectivity studies of Bi have not only corroborated previous work,[8] but have also revealed much additional structure. Observations of the series of oscillations associated with the interband transitions between the strongly coupled electron and valence bands have been extended to higher fields. Oscillations have been observed for the first time with the magnetic field along the trigonal direction. Furthermore, an anomaly has been found in the relative amplitudes of the oscillations associated with the lowest interband transition. In the binary direction, many of the oscillations exhibit weak "satellite" structure which has been identified with "forbidden transitions" of the main series. In addition, oscillations due to a second set of interband transitions have been observed with H parallel to both the binary and bisectrix directions. The energy gap for this series is in good agreement with the value of $E_g = 0.169$ eV

† National Magnet Laboratory, M.I.T.

‡ This experiment was carried out using the high field facilities of the National Magnet Laboratory, M.I.T.

reported by Esaki and Stiles[9] using electron tunneling spectroscopy. Oscillations due to the optical de Haas-Shubnikov effect have been found for H parallel to the binary direction.

Mildred S. Dresselhaus
M. S. Maltz†

7. Infrared Laser High-Resolution Magnetospectroscopy in Graphite‡

A high-resolution magnetospectrometer using a Ne gas laser source has been constructed for application to infrared spectroscopy of solids. This laser oscillates simultaneously at several wavelengths in the range $3\,\mu < \lambda < 22\,\mu$; the wavelengths are selected by a low-resolution monochromator. A balanced optical system reduces the effects of output power fluctuations which are normally severe in infrared lasers. This system has been applied to a study of the low quantum number interband Landau level transitions in graphite for fields $\leqslant 100$ kG. Substantial improvement in resolution, line shape, and signal-to-noise ratio over conventional sources has been achieved by virtue of the inherently small line width and increased power of the source; further improvement results from the laser's greater focusing capability, which effectively eliminates magnetic field inhomogeneities. Considerable fine structure has been observed which has been found to be sensitive to circular polarization.

Mildred S. Dresselhaus
J. G. Mavroides
P. R. Schroeder§
A. Javan§

8. Magnetoplasma Cyclotron Resonance in PbSe

Experimental curves obtained previously[10] for the derivative of the microwave surface absorption at 70 GHz vs static magnetic field of p-PbSe with 1.1×10^{18} holes/cm have been compared with the predictions of the theory of absorption by a high-density plasma under classical skin effect conditions. In the theory, the absorption is calculated from the solution of the wave equation for a plane wave incident on a semi-infinite sample from the left. The complex effective dielectric tensor is calculated assuming a local relation between the current and the electric field, with a $\langle 111 \rangle$ ellipsoidal model for the band extrema and an isotropic, constant carrier relaxation time.

Figure IV-9 shows the results of a machine calculation of the derivative of the absorption compared with the experimentally determined curves; here, the static magnetic field B is aligned along the [100] crystallographic axis. Figure IV-10 presents similar results for B parallel to the [110] axis. In each case, the behavior with the ordinary ($E \parallel B$) and extraordinary ($E \perp B$) modes of propagation, independently excited, is indicated. The close agreement is a verification of the classical skin effect theory and allows a comparatively accurate determination of the valence band effective mass parameters. Best fit is obtained with a transverse effective mass of $m_t = (0.0465 \pm 0.0015)m_o$ and an anisotropy ratio of $K \equiv m_\ell/m_t = 1.8 \pm 0.2$. These values are in satisfactory agreement with the results of Shubnikov-de Haas measurements on PbSe.[11,12]

---

† Department of Electrical Engineering, M.I.T.

‡ This experiment was carried out using the high field facilities of the National Magnet Laboratory, M.I.T.

§ Department of Physics, M.I.T.

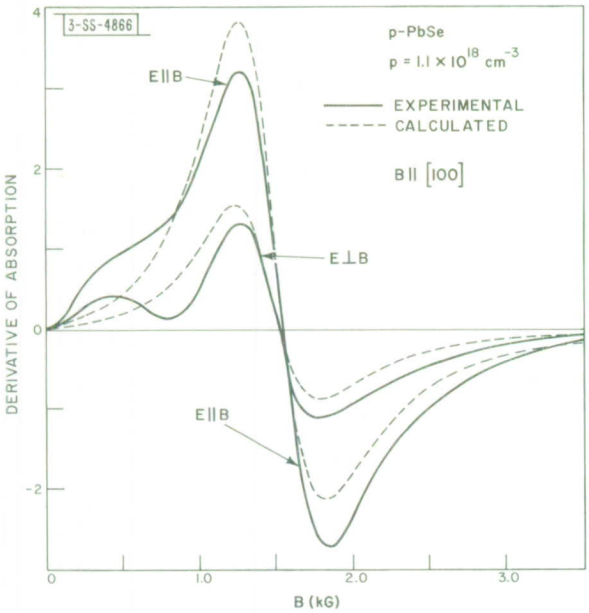

Fig. IV-9. Calculated and experimental plots of derivative of microwave surface absorption vs static magnetic field in p-PbSe with B along [100] axis. Ordinary (E || B) and extraordinary (E ⊥ B) modes shown separately.

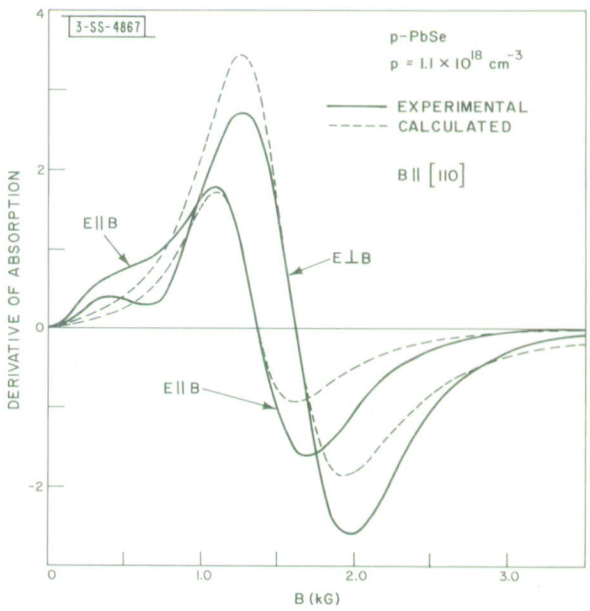

Fig. IV-10. Calculated and experimental plots of derivative of microwave surface absorption vs static magnetic field in p-PbSe with B along [110] axis. Ordinary (E || B) and extraordinary (E ⊥ B) modes shown separately.

The weaker absorption evident at low fields where the cyclotron radius is appreciably greater than the skin depth can probably be attributed to nonlocal effects, such as subharmonics of Azbel'-Kaner resonance. Such effects, of course, cannot be treated within the context of the classical skin effect theory.

Similar resonance behavior has also been observed in a sample of n-PbSe with a carrier concentration of 3×10^{17} electrons/cm^3. The curves are being analyzed and should lead to a determination of the effective mass parameters for the conduction band.

S. Bermon
W. C. Kernan

9. Band Structure of TiO in Tight-Binding Approximation

The tight-binding theory has been used as an interpolation scheme[13] to approximate the energy band structure of TiO as determined by the augmented plane wave (APW) method.[14] Taking account of interactions between nearest and next-nearest neighbors in the rock-salt lattice, a 10×10 secular determinant was set up using Löwdin-type basis functions derived from the 3d and 4s wave functions of titanium and from the 2s and 2p wave functions of oxygen. For special symmetry directions in k-space, it was possible to factor this determinant into subdeterminants by group theoretical considerations. Simple numerical curve-fitting methods were employed to determine the parameters appearing in 1×1 and 2×2 subdeterminants. Bands corresponding to these parametric determinations were then obtained using the tight-binding scheme. The results were found to agree very well with those specified by the APW method. However, it was found that all attempts to reduce the 3×3, 4×4, or 5×5 subdeterminants into simpler forms by use of approximations led to inconsistencies. Therefore, the remaining parameters must be obtained by computer calculations which are being planned for the near future.

Numerical values for the transfer integrals determined so far are as follows in the notation of Ref. 13:

$$E_{xy,\,xy}(000) = 0.636\ \text{ry} \qquad E_{x,\,x}(000) = 0.0980\ \text{ry}$$

$$E_{xy,\,xy}(110) = -0.0155\ \text{ry} \qquad E_{x,\,x}(110) = 0.0131\ \text{ry}$$

$$E_{xy,\,xy}(011) = 0.0157\ \text{ry} \qquad E_{x,\,x}(011) = -0.0080\ \text{ry}$$

$$E_{xy,\,x}(010) = 0.065\ \text{ry} \qquad E_{x,\,y}(110) = -0.016\ \text{ry}$$

J. M. Honig
J. O. Dimmock

10. Fermi Surface, Magnetic Ordering, and Electrical Properties of Thulium Metal

The complete Fermi surface of thulium metal has been determined from a nonrelativistic APW energy band calculation. Computed energy bands are of mixed s-d character and strongly resemble those of the transition metals in this aspect. The computed Fermi surface is determined largely by the d-bands and bears no resemblance to that of the free electron model. The striking anomalies which occur in the c-axis resistivity of the heavy rare-earth metals at the

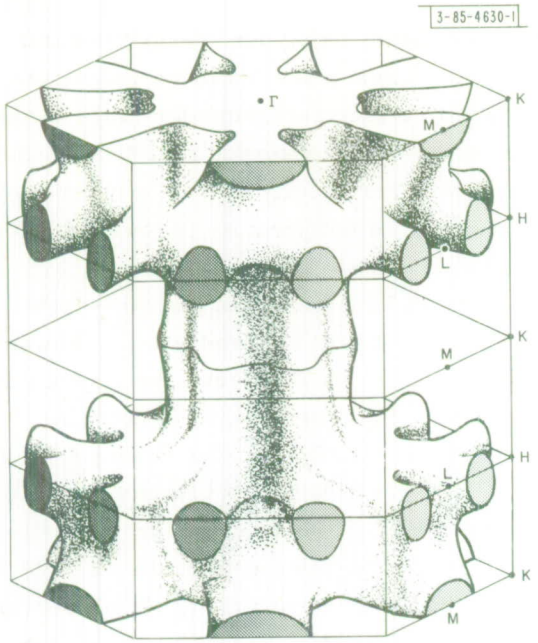

Fig. IV-11. Complete Fermi surface for holes in thulium metal in double zone representation.

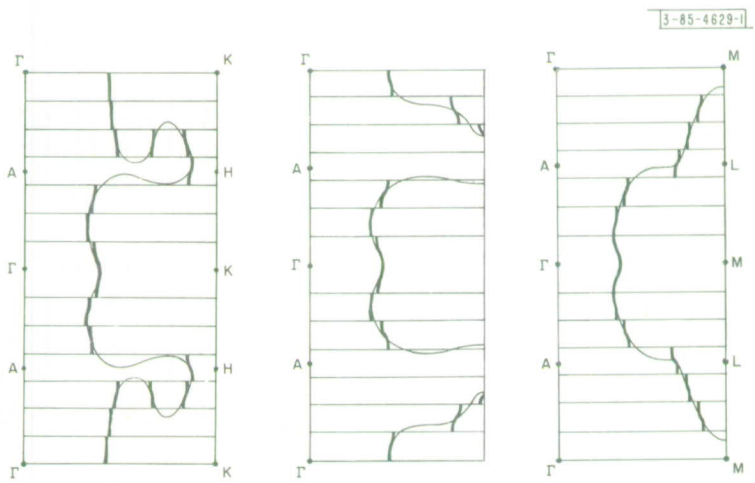

Fig. IV-12. Some vertical cross sections of thulium Fermi surface containing c-axis. Influence of magnetic ordering is demonstrated by comparing low-temperature cross sections (heavy solid curves) with high-temperature cross sections (light solid curves). Horizontal lines denote superzone boundaries at $k_z = \pm n2\pi/7c$ introduced by the magnetic ordering.

onset of long-range periodic magnetic order are understandable, using our energy band and Fermi surface results. We find that the observed $\vec{q}$ vector spans a section of the calculated Fermi surface of thulium such that a section of this Fermi surface perpendicular to the z-axis is destroyed at the onset of magnetic ordering. This results in the observed resistivity anomaly at T_N. Also, because the energy bands are relatively flat in the vicinity of the Fermi energy, sizable gaps occur at superzone boundaries for $k_z = \pm\frac{1}{2}nq$ as the temperature is lowered below T_N, thereby destroying large sections of the Fermi surface normal to the z-axis.

Anomalies in the temperature dependence of the electrical resistivity of the rare-earth metals[15] have been successfully interpreted by Mackintosh,[16] Elliott and Wedgwood,[17] Miwa,[18] and others in terms of the magnetic ordering of these materials. In this view, the anomaly in the electrical resistivity along the c-axis, which occurs at the antiferromagnetic ordering temperature, is associated with band gaps introduced by superzone boundaries arising from the onset of the long-range periodic magnetic order. Good agreement has been obtained between theory and experiment using the free electron model of the conduction bands and the associated Fermi surface. This agreement has since been taken as evidence in support of the validity of the free electron model. However, the recent determination,[19] by means of APW calculations, that the conduction bands in Gd resemble those of the transition metals and differ markedly from free electron bands showed that this model was completely invalid for the rare-earth metals. At the same time, it also raised the question whether agreement between theory and experiment could be restored using the APW band structure and the resulting Fermi surface.

Thulium shows a linear spin wave structure between 50 ° and 40 °K in which the magnitude of the z-component of the moments varies sinusoidally with distance along the c-axis. The period of the wave vector is constant at seven (hexagonal) layers over the observed temperature range. This periodic magnetic structure introduces planes of energy discontinuity (superzone gaps) into the nonmagnetic Brillouin zone structure.[16-18] These energy gaps may affect drastically the electrical conduction of the metal as the temperature is lowered through the Néel temperature, provided one of these superzone boundaries destroys a large part of the Fermi surface.

The complete hole surface for thulium metal determined from our APW calculations is shown in Fig. IV-11. We use the double zone representation which is valid for the cph structure in the absence of spin-orbit coupling. Figure IV-12 presents several vertical cross sections of the Fermi surface. The horizontal lines denote superzone boundaries at $k_z = \pm n2\pi/7c$ introduced by the periodic magnetic ordering. The expected distortion of the Fermi surface at T = 0 is indicated approximately by the heavy solid curves. This effect is a direct consequence of the presence of several relatively flat d-bands in the vicinity of the Fermi energy and would not occur to any extent in the free electron model. The essential feature of the result is that, in the magnetic state, the Fermi surface normal to the z-axis is largely destroyed while segments parallel to the axis remain, though somewhat perturbed. This implies a resistance anomaly parallel but not perpendicular to the crystal c-axis in agreement with experiment. It should be pointed out, however, that the calculations we have performed are all nonrelativistic and that relativistic corrections, including spin-orbit effects, will certainly modify to some extent the computed Fermi surface. Nevertheless, we feel that the general features of the Fermi surface

(as shown in Fig. IV-11) and of the effects of magnetic ordering (as shown in Fig. IV-12) should remain even when the relativistic effects are taken into account. It thus appears that the anomalies in the temperature dependence of the resistivity of the heavy rare-earth metals can be understood in terms of the calculated energy bands of these materials, and that qualitative agreement, at least, exists between theory and experiment.

J. O. Dimmock
A. J. Freeman†
R. E. Watson‡

11. Polaron Landau Levels

The second order Rayleigh-Schrödinger perturbation correction to the n = 1 Landau level energy of conduction band electrons interacting with the longitudinal optical phonons of a polar crystal has been investigated recently.[20] It was found that the perturbation correction diverges as the energy separation $\hbar\omega_c$ between the unperturbed n = 1 and 0 levels approaches $\hbar\omega_o$, the longitudinal optical phonon energy, from below. This result suggests that, in reality, relatively pronounced polaron effects on the n = 1 level should be observed when the applied magnetic field is strong enough to force the energy difference between the n = 1 and 0 polaron Landau levels to approach $\hbar\omega_o$. Therefore, it is of some interest to study the behavior of the n = 1 level as a function of magnetic field.

If we calculate the energy of the n = 1 level by second order Wigner-Brillouin perturbation theory, we find that, while the energy obtained [$E_{WB}(\omega_c)$] is a monotonically increasing function of magnetic field, $dE_{WB}(\omega_c)/d\omega_c$ decreases sharply as $\omega_c \to \infty$. However, it is doubtful that the perturbation theory is valid for ω_c much greater than ω_o.

To improve on perturbation theory, the variational method for free polarons (no magnetic field) described recently[21] has been generalized to the case in which a magnetic field is present. The energy band by this technique for the n = 1 Landau level will be denoted E_v. Numerical computations show that the approximately linear low-field behavior of E_v is destroyed at higher fields, where $dE_v/d\omega_c$ becomes very small.

One expects that the exact energy difference between the n = 1 and 0 levels should approach $\hbar\omega_o$ as $\omega_c \to \infty$. This condition is fulfilled only approximately in Wigner-Brillouin perturbation theory and in the above-mentioned variational theory. Attempts to improve the variational method are under way.

Finally, study of the approximate weak-coupling wave function for the polaron indicates that the probability of exciting a polaron in the n = 1 level by shining radiation on the crystal begins to decrease markedly with increasing ω_c when ω_c exceeds ω_o.

D. M. Larsen

---

† National Magnet Laboratory, M.I.T.

‡ Brookhaven National Laboratory, Upton, Long Island, New York.

B. HYPERSONIC WAVES IN SOLIDS

1. Temperature Dependence of 70-GHz Transverse Acoustic Waves

Experimental measurement of the temperature dependence of 70-GHz acoustic waves in quartz, using a pulse-echo technique, has been extended to include transverse waves in BC-cut quartz. The results are shown in Fig. IV-13, along with values previously measured for longitudinal waves in x-cut quartz. The T^4 dependence, as well as the absolute value of the attenuation, is seen to be the same for both modes down to 10 °K. Measurements below 10 °K were not useful because of the large fractional uncertainty in the measured temperature-dependent attenuation, caused by the presence of a temperature-independent background equivalent to about 2 dB/cm, which ultimately limited the number of observable echoes. Attenuation of the transverse phonons follows the theory of Landau and Rumer in terms of a three-phonon interaction of the coherent wave with thermal phonons through anharmonic terms in the elastic energy. The observed temperature dependence of the longitudinal attenuation can be explained in this same framework if the momentum conservation is relaxed, as permitted by the short lifetime of the thermal phonons. Recent experiments[22] at lower frequencies have indicated, and theories have been proposed[23] to explain, an increasing exponential dependence of longitudinal attenuation at low temperature in Al_2O_3. It was proposed that the increasing rate is a consequence of the gradual failure of the thermal phonon energy uncertainty to overcome the conservation requirements with decreasing temperature.

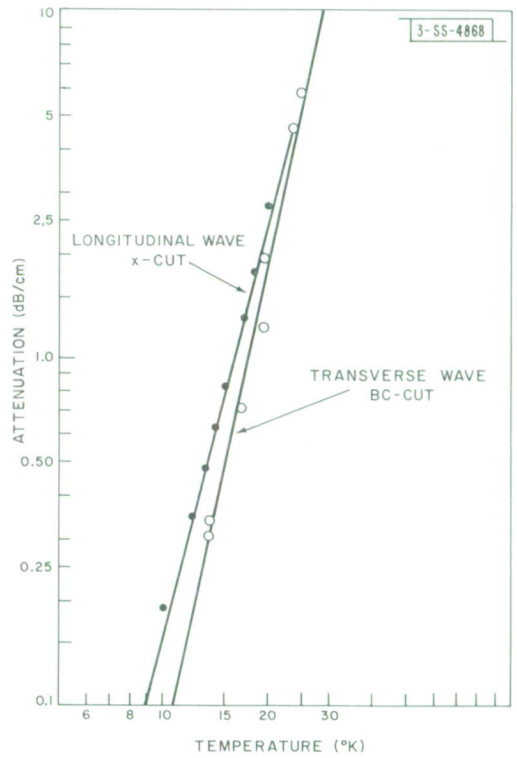

Fig. IV-13. Comparison of temperature dependence of 70-GHz longitudinal and transverse waves in a-quartz.

TABLE IV-1

EXPERIMENTAL COMPARISON OF TRANSDUCTION EFFICIENCIES IN TERMS OF INSERTION LOSS

Material	Frequency	Mode	Transducer	Insertion Loss (dB)
Al (poly)	34 MHz	L†	34 MHz x-plate	42
	35 MHz	L	62 μ CdS	22
	10 MHz	T‡	10 MHz y-plate	44
	14 MHz	T	62 μ CdS	22
Permalloy (poly)	33 MHz	L	34 MHz x-plate	61
	41 MHz	L	54 μ CdS	38
	10 MHz	T	10 MHz y-plate	69
	16 MHz	T	54 μ CdS	36
x-quartz	85 MHz	L	Surface	69
	85 MHz	L	25 μ CdS	47
Al_2O_3 c-axis along rod	1 GHz	L	2.2 μ CdS	38
Ruby a-axis along rod	1 GHz	L	2.2 μ CdS	47
	1 GHz	T	2.2 μ CdS	51
	1 GHz	T	2.2 μ CdS	60
x-quartz	1 GHz	L	Surface	60
	1 GHz	L	2.2 μ CdS	42
x-quartz	9 GHz	L	Surface	93
	9 GHz	L	1.7 μ CdS	64
z-quartz	9 GHz	L	1.7 μ CdS	59
GaAs, InSb	9 GHz	L	1.7 μ CdS	–
z-quartz	70 GHz	L	0.1 and 0.16 μ CdS	–

† Longitudinal

‡ Transverse

In our measurements, no increase in the attenuation rate was observed in quartz for 70-GHz phonons down to 10 °K. An additional factor that must be considered in the 70-GHz experiment is that the condition $\hbar\omega \sim kT$ is now being approached, especially at low temperatures; thus, additional attenuation processes become allowed.

J. B. Thaxter
C. D. Parker

2. Some Comparative Data on CdS Transducers from 14 MHz to 70 GHz

As mentioned in a previous Solid State Research Report,[24] insulating piezoelectric CdS film transducers have been deposited on metallic, nonmetallic, and semiconducting materials using a simple electron-bombardment technique. The electromagnetic frequency range of excitation of the phonon spectra has varied from 14 MHz on aluminum, to 70 GHz on z-cut quartz. Data have now been obtained by pulse-echo techniques† which allow in some instances comparisons to be made between the performance of these transducers and other methods of acoustic excitation commonly used in the same situation; e.g., for metals, comparison is made with resonant quartz plates bonded to the end faces, while for piezoelectric materials, comparison is made with surface generation. Comparisons are for the same material under nearly identical experimental conditions with respect to the geometry of excitation, electrical matching, temperature, and frequency.

The measured quantity of major importance is the insertion loss. This is the difference in RF power levels between the initial incident pulse and the first returning echo less the attenuation in the medium for one complete trip of the sound packet. To assure meaningful results, the megahertz measurements were made using fixed-tuning broad-band structures which resulted in bandwidths in excess of 50 percent. In the gigahertz range, conventional re-entrant cavity techniques were used, resulting in bandwidths of the order of 20 percent. Over both ranges, the mode of excitation was determined by the orientation of the exciting electric field with respect to the plane of the transducer, which, in turn, was determined by the special geometrical shapes of the electrodes. It should be pointed out that the insertion loss measurements in the gigahertz region are inordinately high because of the inefficient use of the exciting electric field. Thus, comparisons are even more useful in this case.

Table IV-1 presents comparisons in terms of insertion losses for appropriate pairs of measurements. The temperature was generally 300 °K except for the measurements above 1 GHz, which were made at 4.2 °K. The transducers were in the form of $\frac{1}{4}$-inch disks whenever possible. From 9 to 70 GHz, the CdS transducers were excited at frequencies ranging from the 3rd to the 7th harmonic.

The following definite conclusions can be drawn from these results.

(a) Piezoelectric, high-resistivity ($\approx 10^8$-ohm-cm) CdS transducers can be vapor deposited in a reproducible fashion onto metallic, nonmetallic, and semiconducting media. The purity of the longitudinal mode excited in correct geometries indicates that the transducer c-axis is closely perpendicular to the plane of the transducer. Moreover, for single crystals and for certain polycrystalline materials, the deposited CdS films are sufficiently oriented in the plane to also provide efficient excitation of the transverse mode.

†K. W. Nill performed the X-band measurements; J. B. Thaxter and C. D. Parker performed the measurements at 70 GHz.

(b) Even though it was necessary to make successive depositions to obtain thick films (because of the limited capacity of the apparatus), there is still a substantial decrease in the insertion loss to be obtained by use of these transducers as opposed to the use of bonded resonant quartz plates operating on their fundamental frequencies. (Surprisingly, there was no peeling or deterioration of the thick, layered CdS transducers as they were cycled between room temperature and 4.2 °K.)

(c) From 14 MHz to 9 GHz, the CdS transducers have shown decidedly superior insertion loss characteristics (≈20-dB improvement) when compared with other common means of excitation in similar configurations.

(d) Transducers of the order of 0.1-μ thickness deposited on z-cut quartz have been found to be active by cavity excitation at 70 GHz.

R. Weber

3. Microwave Phonon Generation at 24 and 70 GHz Using CdS Thin-Film Transducers

Tests to determine the relative transduction efficiency of vapor-deposited thin-film CdS transducers† were made at both 24 and 70 GHz. The transduction efficiency at 24 GHz of several films, acoustically nonresonant in thickness and deposited on quartz substrates, was comparable to the efficiency observed for single-surface generation in x-cut quartz. At 70 GHz, the CdS film transducers tested on z-cut quartz substrates are not so efficient as x-cut quartz. The above results, taken together with the findings of others at lower frequencies, indicate that there is a trend for the relative transduction efficiency of the CdS to decrease at the higher frequencies. One possible reason for this could be roughness of the substrate surface, which would tend to inhibit the initially deposited layer from having a good crystalline structure.

Attempts to detect 70-GHz phonon echoes in Al_2O_3 using CdS transducers have not been successful. Close examination of the surface of the substrate reveals work marks, characteristic of polished sapphire, in the form of scratches 250 Å deep, which correspond to $\lambda/6$ of the acoustic wave. MgO substrates, which can provide surfaces of high optical quality, are being prepared for use at 70 GHz.

J. B. Thaxter
C. D. Parker

C. MAGNETISM

1. Classical Ground Spin States in Normal Cubic Spinels with Nonmagnetic A-Sites

Ferromagnetic $CdCr_2Se_4$ and antiferromagnetic $ZnCr_2Se_4$ are both spinels with nonmagnetic ions on their A-sites.[25] They both possess strongly ferromagnetic nearest-neighbor Cr-Se-Cr 90° superexchange interactions. Weaker, antiferromagnetic next-nearest-neighbor Cr-Se-Se-Cr interactions can play a decisive role in determining the type of long-range magnetic order, but the extent to which these interactions are influenced by the A-site cation is not yet known.[25]

In an attempt to answer this question, we have begun a theoretical investigation of the classical ground spin state in these materials. The classical Heisenberg energy is given by

† These films were prepared by R. Weber and J. W. Burke (see Sec. IV-B-2).

$$E = -\sum_{n\nu,\, m\mu} \bar{J}_{n\nu,\, m\mu} \vec{S}_{n\nu} \cdot \vec{S}_{m\mu} = -\bar{J} \sum_{n\nu,\, m\mu} \mathcal{J}_{n\nu,\, m\mu} \vec{S}_{n\nu} \cdot \vec{S}_{m\mu} \tag{4}$$

where $\vec{S}_{n\nu}$ is a unit vector in the direction of the spin on the $n\nu^{th}$ site, n runs over the unit cells in the sample, ν runs over the four different B-sites within each unit cell, the $\bar{J}_{n\nu,\, m\mu}$ are the usual exchange integrals (>0 when ferromagnetic) multiplied by the magnitudes of the spins, $\bar{J}$ is the dominant nearest-neighbor interaction, and the $\mathcal{J}_{n\nu,\, m\mu}$ are ratios of the other interactions to $\bar{J}$. It is convenient to work with the Fourier transform of Eq. (4),[26]

$$E = -2N\bar{J} \sum_{\vec{k}} \sum_{\nu\mu} L'_{\nu\mu}(\vec{k})\, \vec{Q}^{*}_{\nu}(\vec{k}) \cdot Q_{\mu}(\vec{k}) \tag{5}$$

where

$$\vec{S}_{n\nu} = \sum_{\vec{k}} \vec{Q}_{\nu}(\vec{k}) \exp[i\vec{k} \cdot \vec{R}_{n\nu}] \tag{6}$$

$$L'_{\nu\mu}(\vec{k}) = \frac{1}{2} \sum_{m} \mathcal{J}_{n\nu,\, m\mu} \exp[i\vec{k} \cdot (\vec{R}_{m\mu} - \vec{R}_{n\nu})] \quad . \tag{7}$$

We shall use the notation $\vec{k} = (2\pi/a_o)$ (h, k, ℓ) for vectors in reciprocal space, and $\vec{R} = (a_o/4)$ (r, s, t) for vectors in real space, a_o being the usual cell edge. Thus, $\vec{R}_{n\nu} = \vec{R}_n + \vec{\rho}_\nu$, where the lattice vector $\vec{R}_n$ is expressed in terms of the basic face-centered translations (2, 2, 0), (2, 0, 2), and (0, 2, 2), and where the four B-sites in the unit cell occupy the positions $\vec{\rho}_\nu$ = (1, 0, 1), (0, 1, 1), (0, 0, 0), and (1, 1, 0) as ν runs from 1 to 4.

It is clear from Eq. (4) that the configuration of spin vectors which minimizes the energy depends only on the $\mathcal{J}_{n\nu,\, m\mu}$, i.e., on the ratios of the next-nearest-neighbor interactions to the nearest-neighbor exchange $\bar{J}$. Here, the class of next-nearest-neighbor interactions is taken to include <u>all</u> superexchange linkages of the form Cr-Se-Se-Cr, regardless of the actual distance between the endpoints. The problem is difficult because of the variety of such linkages in the spinel lattice. Some of the distinct types of linkages are illustrated in Fig. IV-14. For example, the lower left-hand corner of this figure shows a σ-Se-Se-σ and a π-Se-Se-π path, both linking a B_4 site with another B_4 such that $\vec{\tau}^{\,m\mu}_{n\mu} = \vec{R}_{m\mu} - \vec{R}_{n\mu}$ = (2, 2, 0) for μ = 4. Since these two paths are inseparable, they are lumped together under the designation U. This linkage U occurs twice (once as shown in Fig. IV-14 and again with the roles of the σ- and π-anions reversed), so that the total superexchange interaction associated with this $\vec{\tau}^{\,m\mu}_{n\mu}$ is 2U. As shown in the upper left-hand corner, a similar total superexchange interaction of 2V is associated with a $\vec{\tau}^{\,m\mu}_{n\mu}$ = ($\bar{2}$, 2, 0) for μ = 3. The linkage V differs from U only in that its two anions share an A-site. If their interaction with this A-site ion were negligible, then V would equal U.

A σ-Se-Se-π linkage between a B_3 and a B_4 with $\vec{\tau}^{\,m\mu}_{n\nu}$ = (1, $\bar{3}$, 0) is illustrated in the upper right-hand corner of Fig. IV-14. This interaction X is taken to include the interchange of the σ- and π-anion roles. These anions share a common A-site, and X = V in the limit where the superexchange occurs via the A-site cation. The total exchange interaction for the (2, 1, 1) family of $\vec{\tau}^{\,m\mu}_{n\nu}$ is more complicated. It consists of two σ-Se-Se-π links which share an A-site,

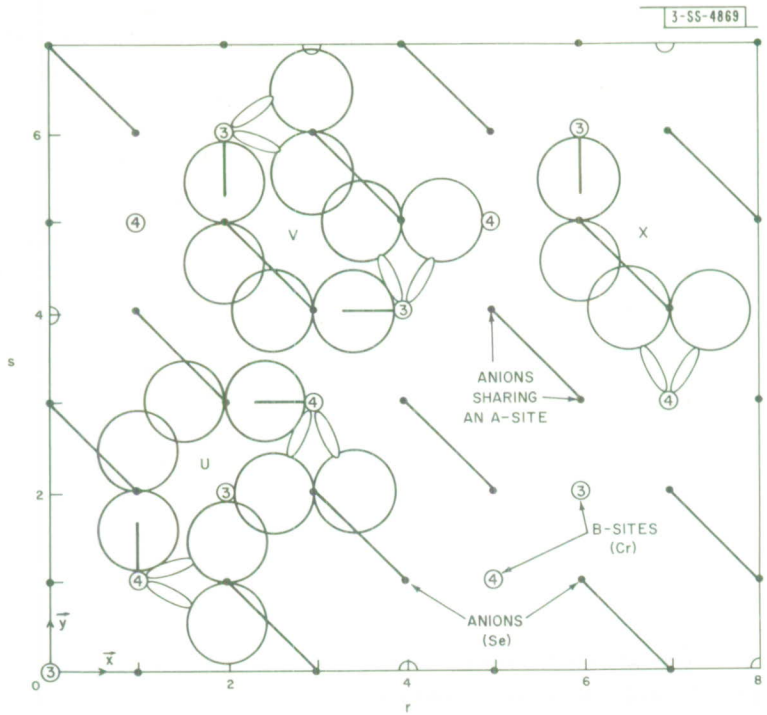

Fig. IV-14. Cr-Se-Se-Cr superexchange linkages in the (r,s,0) plane of a selenio-chromite spinel.

plus two which do not, plus two π-Se-Se-π links which share an A-site, plus four which do not. Let 2W denote the sum of all these effects.

Given the above definitions, one obtains for

$$\vec{k} = \frac{2\pi}{a_o}(0, 0, h)$$

$$L'_{\mu\mu}(h) = 2(U + V) + 4(U + V)\cos 2\sigma \quad , \quad \text{for all } \mu$$

$$L'_{12}(h) = L'_{14}(h) = (1 + 2X) + 4W \cos 2\sigma$$

$$L'_{13}(h) = L'_{14}(h) = L'_{23}(h) = L'_{24}(h) = (1 + 4W + X)\cos\sigma + X \cos 3\sigma$$

$$L'_{\nu\mu}(h) = L'_{\mu\nu}(h) \qquad (8)$$

where $\sigma = \pi h/2$. This matrix can be diagonalized by inspection to give

$$\lambda'_1(\sigma) = (1 + 2U + 2V + 2X) + (2 + 2X + 8W)\cos\sigma$$
$$+ 4(U + V + W)\cos 2\sigma + 2X \cos 3\sigma$$

$$\lambda'_2(\sigma) = \lambda'_3(\sigma) = (-1 + 2U + 2V - 2X) + 4(U + V - W)\cos 2\sigma$$

$$\lambda'_4(\sigma) = \lambda'_1(\pi - \sigma) \quad . \qquad (9)$$

The corresponding eigenvectors $\Psi_\alpha(\sigma)$ are, respectively, $1/2(1, 1, 1, 1)$, $1/\sqrt{2}(1, -1, 0, 0)$, $1/\sqrt{2}(0, 0, 1, -1)$, and $1/2(1, 1, -1, -1)$. The first of these, $\Psi_1(\sigma)$, describes the ferromagnetic

state when $\sigma = 0$. According to Eq. (9), this can be the ground state, i.e., the minimum Heisenberg energy, only when its eigenvalue $\lambda_1(0)$ is the maximum (over both α and σ) of the above eigenvalues. Thus, one finds that

$$1 + 8U + 8V + 12W - 2X \geqslant 0 \tag{10}$$

$$1 + 4W + 2X \geqslant 0 \tag{11}$$

$$1 + 2U + 2V + 2W + 2X \geqslant 0 \tag{12}$$

are necessary conditions for ferromagnetism. These equations place rather stringent restrictions on the possible magnitude of the next-nearest-neighbor interactions in $CdCr_2Se_4$.

For values of the exchange parameters U, V, W, and X which satsify Eqs. (11) and (12), but not Eq. (10), $\lambda_1'(\sigma)$ is maximum for a finite value of σ. Then, $\lambda_1'(\sigma)$ corresponds to a (0, 0, 1) spiral of the type observed in $ZnCr_2Se_4$.[27] A detailed investigation of this region of the parameter space is in progress.

K. Dwight
N. Menyuk

2. Magnetic Resonance Measurements on $CdCr_2S_4$

Preliminary X-band magnetic resonance line-width measurements on polycrystalline $CdCr_2S_4$, prepared by A. Wold of Brown University, have been made as a function of temperature from 4.2° to 295°K. The line width decreases from approximately 700 Oe at 4.2°K to 420 Oe at 71°K, at which point there is a sharp decrease to 85 Oe at 106°K. Then the line width remains essentially constant at 85 Oe up to 295°K. This qualitative behavior of the temperature dependence of the line width is in agreement with the susceptibility measurements of Menyuk, et al.,[28] who found a Curie temperature of 86°K. The increasing line width with decreasing temperature below the Curie point is presumably attributable to magnetocrystalline anisotropy of the sample. The point of interest in studying the line width in ferromagnetic chalcogenides such as $CdCr_2S_4$ is that these materials are ferromagnetic spinels which have, in contrast to the well-known ferrites, an ordered structure, and hence might be expected to exhibit a narrow ferromagnetic resonance line width. The possibility of preparing and measuring single crystals is being explored.

R. Weber
P. E. Tannenwald
J. W. Burke

3. Magnon Dispersion Relation

In a previous Solid State Research Report,[29] Marshall's model-independent argument was used (a) to predict the temperature dependence of the magnon dispersion relation

$$\epsilon_k = D_o(1 - GT^{5/2} + LT^{7/2} + \ldots)\, k^2 - F_o(1 - HT^{5/2} + \ldots)\, k^4 + \ldots \tag{13}$$

and (b) to relate G, H, and L. We have since obtained explicit expressions for these coefficients for the case of the Heisenberg model.[30]

We also found that the ratio H/G is surprisingly simple:

$$\frac{H}{G} = \frac{\langle r^6 \rangle}{[\langle r^4 \rangle]^2} \tag{14}$$

where $\langle r^{\ell} \rangle = \sum_r r^{\ell} J(r) / \sum_r r^2 J(r)$. Now, $\langle r^{\ell} \rangle$ is proportional to the temperature-independent coefficient of the k^{ℓ} term in the dispersion relation [Eq. (13)], which has been recently measured[31] through order k^6 for Fe by inelastic neutron scattering. The value for the right-hand side of Eq. (14), calculated[32] from these neutron data on Fe, are in order-of-magnitude agreement with the value of H/G obtained from spin wave resonance experiments[33] on 63% Ni-37% Fe permalloy film, providing a crude check on these predictions based on the Heisenberg model. Tentative arrangements are being made[34] to take all the pertinent measurements on the same material.

H. E. Stanley
T. A. Kaplan

4. Space-Time Symmetry Restrictions on Transport Coefficients – Comparison of Two Theories

The space-time symmetry restrictions on transport coefficients given by two recent theories[35,36] have been compared and the differences exhibited in detail for the zero-magnetic-field electrical conductivity. The symmetry restrictions of one of the theories[35] have been shown to be inconsistent with the existence of the extraordinary Hall effect in ferromagnets.

W. H. Kleiner

D. NONLINEAR OPTICS

1. Stimulated Raman Scattering in Quartz

Experiments previously reported† in quartz have been extended to low temperatures. Samples are mounted on the end of a cold finger in a vacuum chamber of a helium dewar. The sample temperature is estimated to be 10° to 15°K. The ~200-MW ruby laser beam is focused by an external lens onto the sample through a fused quartz window in the dewar, and the scattered radiation is detected about the forward direction through a similar window.

Compared with room-temperature operation, the threshold at low temperatures for stimulated Brillouin scattering is only slightly lower, while there is a significant reduction for stimulated Raman emission, presumably because the spontaneous line is narrower. Since there is only slight sample damage, many repeated measurements can be made. The following stimulated shifts were observed:

$S_1 = 463\ cm^{-1}$ $\quad AS_1 = 469\ cm^{-1}$

$S_2 = 2 \times 466\ cm^{-1}$ $\quad AS_2 = 2 \times 468\ cm^{-1}$

$S_3 = 3 \times 466\ cm^{-1}$ $\quad AS_3 = 3 \times 467\ cm^{-1}$

$S_4 = 4 \times 466\ cm^{-1}$ $\quad AS_4 = 4 \times 467\ cm^{-1}$

$S_5 = 5 \times 467\ cm^{-1}$

† Solid State Research Report, Lincoln Laboratory, M.I.T. (1965:3), p. 18, DDC 629048.

In addition to the 466-cm^{-1} line and its multiples, the very strong 128-cm^{-1} line of the classical Raman spectrum of quartz belonging to the doubly degenerate class E was observed, but only when the laser beam (propagating along the x-axis) was polarized perpendicular to the c-axis. This agrees with the selection rule $\epsilon_{zz} = 0$, where ϵ_{ik} are the components of the Raman scattering tensor. The scattered radiation was strongly polarized so that, of the allowed transitions, ϵ_{yy} is strong and ϵ_{yz} must be weak. A variety of combination lines was generated, as shown in Fig. IV-15, with the actual wave-number shifts at low temperature averaging near 132 cm^{-1}.

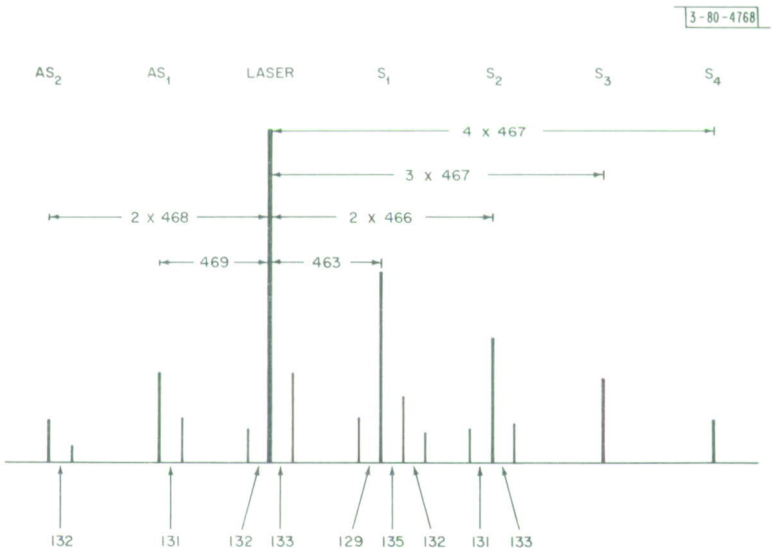

Fig. IV-15. Multiple shifts and combination lines occurring in stimulated Raman spectrum of quartz. All shifts are in cm^{-1}.

A rough mapping out of the angular distribution of the 466-cm^{-1} stimulated Raman radiation up to 15° showed that all lines peak up in the forward direction. This is expected from the very small dispersion of quartz in this part of the spectrum and the phase-matching condition. The absence of an additional angular peak in AS_1 radiation, in which phase-matched extraordinary AS_1 radiation is excited from incident laser radiation polarized as an ordinary ray, follows the selection rule $\epsilon_{ik} = 0$ for the totally symmetric class A vibration.

P. E. Tannenwald
F. H. Perry

2. Temperature Dependence of Incoherent Second Harmonic Light Scattering in Liquids

The incoherent second harmonic scattering[37] in water of a ruby laser beam increases approximately linearly with decreasing temperature, below room temperature, and has about doubled at 8 °C as shown in Fig. IV-16. The measurements were undertaken in order to study the intermolecular orientation correlations in liquids. It was deduced from the symmetry of the second harmonic polarizability tensor that the undisplaced component of scattering arises only from orientation fluctuations, rather than from density fluctuations. This contrasts with

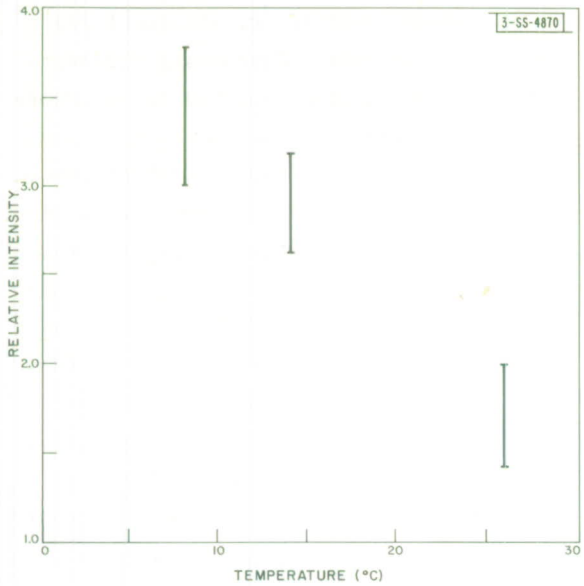

Fig. IV-16. Temperature dependence of incoherent second harmonic scattering intensity in water. Error bars represent standard deviations.

Rayleigh scattering in liquids, which arises almost entirely from density fluctuations, and to that extent depends only on the thermodynamic properties of the liquid. It was expected that changes in the orientation correlations could most easily be observed by varying the temperature. The temperature dependence of the depolarization has not been measured.

Scattering was first detected here with an experimental setup which, although basically similar to that of Terhune, et al.,[37] differed in having a laser pulse duration of less than 20 instead of 80 nsec, a breakdown threshold for water of 0.2 instead of 1 MW, a cylindrical sample cell with a collection lens at f/1.4 (at 90° to the incident beam) instead of a cell of rectangular cross section with a mirror at f/1, and possibly a smaller focal spot. The water used was doubly distilled, conductivity-monitored, and passed through a 0.5-μ pore size Millipore filter into a carefully cleaned cell. The need to operate almost at breakdown threshold, and the output capability of the laser, limited the pulse length and focal spot size. Apparently as a result of these differences, at most two photoelectrons per laser pulse, of second harmonic signal into a 500-cm^{-1} bandwidth, could be obtained (and that only with very careful adjustment) instead of the more than 100 photoelectrons into an 80-cm^{-1} bandwidth found by Terhune, et al.[37] The bandwidth determines the monochromator slit width. Since the laser could be fired only about once every $1\frac{1}{2}$ minutes, a 600-cm^{-1} bandpass filter was substituted for the monochromator in order to collect data at a reasonable rate. (The wavelength of the signal was verified by interchanging it with a similar filter with pass band 350 cm^{-1}, centered 750 cm^{-1} toward longer wavelengths.) Signals of about 20 photoelectrons were then found at room temperature. Coherent second harmonic production in quartz by a small fraction of the beam was used as a monitor, but there was little correlation between the changes in pulse height or shape on the two channels at constant temperature, possibly because the independent modes of the laser pulse combine differently in incoherent and coherent second harmonic generation. The temperature was varied by the rate of flow of cold nitrogen gas over the sample cell, and was measured by two thermocouple junctions near, equidistant from, and on opposite sides of the focal region.

The density maximum in water at 4 °C suggests a two-phase model for its structure, with the denser phase having a higher free energy, and a population therefore increasing with temperature. Hall[38] proposed such a model, perhaps the most often quoted model of the structure of water, in order to account for the measured acoustic attenuation. His model cannot explain the present results, because he deduced a free energy of activation equivalent to 250 °K, while Fig. IV-16 yields 3000 °K. In other words, increasing temperature transfers too few molecules from the low-temperature ordered phase, to the high-temperature disordered phase, to fit our experiment. One may probably say that the region of orientational correlation shrinks rapidly, approaching a single molecule, as water is heated. This suggestion is consistent with the pair distribution of intermolecular distances, found by x-ray diffraction,[39] which should be a valid criterion for associated liquids such as water. For uniform correlation within equal volumes V of single phase liquid, and no correlation among them, the scattering intensity is proportional to V. One then anticipates that nonassociated liquids will show less temperature dependence of second order incoherent light scattering, since they have weaker intermolecular orientational correlation than water.

D. L. Weinberg

3. Possibility of Self-Focusing Due to Nonlinear Anomalous Dispersion

Here we point out that, close to an atomic resonance, the dependence of the real part of the susceptibility on power level (i.e., saturation effects) can be sizable and therefore lead to self-trapping or self-focusing. The details of the self-focusing effect due to a nonlinear increase in index of refraction have been treated elsewhere.[40,41]

For a homogeneously broadened line, the expansion of the well-known formula for the susceptibility as a function of electric field gives a change in index δn proportional to the intensity, i.e.,

$$\delta n = -\frac{2\pi}{n_o}\,\chi'_{res}(\omega)\,\{(\hbar^{-2}\mathcal{P}^2E^2T'^2)\,[1+(\omega-\omega_o)^2\,T^2]^{-1}\} \tag{15}$$

where

$$\chi'_{res}(\omega) = \chi''_{res}(\omega_o)\,(\omega_o-\omega)\,T\,[1+(\omega-\omega_o)^2\,T^2]^{-1} \tag{16}$$

is the real part of the linear susceptibility due to the atomic or molecular resonance. For an inverted system, $\chi'_{res}(\omega)$ is negative on the low-frequency side of the atomic resonance. In Eq. (15), $\mathcal{P}$ is the dipole matrix element, T is the inverse of the line width, ω is the operating frequency, and ω_o is the resonance frequency. T' is a characteristic time which is determined by the lifetimes of the atomic levels and is different for transient as opposed to steady-state response. For an atomic system giving rise to Q-switched or CW laser operation, sizable intensities can be obtained which make the term in braces of the order of unity. Furthermore, the same considerations hold if the system is used as an amplifier operated near saturation. We shall assume that the atomic distribution and the level populations are reasonably homogeneous throughout the region of interest, so that spatial inhomogeneities in the linear index do not obscure the focusing effect.

We note that for a CO_2 laser at moderate pressures, where the line is homogeneously broadened because of collisions, $\delta n \approx 1.2 \times 10^{-6}$ when the gain is a factor of 3 per meter and $(\omega_o - \omega)\, T \approx 1$. For a Q-switched ruby laser operated at room temperature, where the line is predominantly homogeneously broadened, we estimate that for normal pink ruby $\delta n \approx 1.7 \times 10^{-6}$ if $(\omega_o - \omega)\, T \approx 1$.

Self-focusing is possible when

$$\delta n \geqslant \delta n_{cr} \equiv \frac{(1.22\lambda)^2}{8 n_o d^2} \tag{17}$$

where d is the diameter of the beam. Self-trapping occurs when δn takes on its critical value. In practical situations, δn_{cr} is of the order of 10^{-7} so that sizable self-focusing and trapping is likely for the cases mentioned above. These effects might account for the filamentary nature of the output of Q-switched ruby lasers as well as other laser systems, such as semiconductor lasers. According to our analysis, the presence of filamentary structure should be accompanied by operation of the laser on the low-frequency side of the resonance. It should also be mentioned that important effects on the operating characteristics of the laser may occur because self-trapping will lead to propagation through the region where the density of excited atoms is maximum.

For an inhomogeneously broadened line, Eq. (15) is correct provided $|\omega - \omega_o| > \Delta\omega$, where $\Delta\omega$ is the inhomogeneous width. However, within this line in a traveling-wave situation, the index change should be markedly reduced from the homogeneous value by a factor of $(T\Delta\omega)^{-1}$; but, in a gaseous system, the result for the standing-wave case is again similar to Eq. (15) and occurs because of the same effect which leads to the Lamb dip. In this case, expressions (15) and (16) still roughly hold when $|\omega_o - \omega|\, T \leqslant 1$. High-gain CW gas lasers such as Xe laser transitions are likely candidates for the study of the self-focusing effect.

P. L. Kelley
A. Javan†

† Department of Physics, M.I.T.

REFERENCES

1. Solid State Research Report, Lincoln Laboratory, M.I.T. (1965:3), p.37, DDC 629048.
2. H. Ehrenreich and H. Philipp, Phys. Rev. 128, 1622 (1962).
3. Solid State Research Report, Lincoln Laboratory, M.I.T. (1965:3), p.38, DDC 629048.
4. Q.H.F. Vrehen, Phys. Rev. (to be published).
5. G.A. Akhundov, Optics and Spectroscopy 18, 420 (1965).
6. G.A. Akhundov and I.G. Aksyanov, Optics and Spectroscopy 19, 172 (1965).
7. C.R. Pidgeon and R.N. Brown, Bull. Am. Phys. Soc. 11, 52 (1966).
8. R.N. Brown, J.G. Mavroides and B. Lax, Phys. Rev. 129, 2055 (1963).
9. L. Esaki and P.J. Stiles, Phys. Rev. Letters 14, 902 (1965).
10. Solid State Research Report, Lincoln Laboratory, M.I.T. (1965:3), p.42, DDC 629048.
11. K.F. Cuff, M.R. Ellett, C.D. Kuglin and L.R. Williams, Proceedings of the 7th International Conference on the Physics of Semiconductors, Paris, 1964 (Dunod, Paris, 1964), p.677.
12. Solid State Research Report, Lincoln Laboratory, M.I.T. (1965:1), p.74, DDC 622446, H-678.
13. J.C. Slater and G.F. Koster, Phys. Rev. 94, 1498 (1954).
14. V. Ern and A. Switendick, Phys. Rev. 137, A1927 (1965).
15. P.M. Hall, S. Legvold and F. Spedding, Phys. Rev. 109, 971 (1958); R.V. Colvin, S. Legvold and F.H. Spedding, Phys. Rev. 120, 741 (1960); D.E. Hegland, S. Legvold and F.H. Spedding, Phys. Rev. 131, 158 (1963).
16. A.R. Mackintosh, Phys. Rev. Letters 9, 90 (1962).
17. R.J. Elliott and F.A. Wedgwood, Proc. Phys. Soc. (London) 81, 846 (1963).
18. H. Miwa, Progr. Theoret. Phys. (Kyoto) 29, 477 (1963).
19. J.O. Dimmock and A.J. Freeman, Phys. Rev. Letters 13, 750 (1964), DDC 613895.
20. D.M. Larsen, "Cyclotron Resonance of Piezoelectric Polarons," Phys. Rev. (to be published).
21. _____, "Polaron Energy Spectrum," Phys. Rev. (to be published).
22. J. deKlerk, Phys. Rev. 139, A1635 (1965).
23. P.G. Klemens, 1965 IEEE Ultrasonics Symposium, Boston, Mass.; also to be published in Physical Acoustics, Vol. IIIB, edited by W.P. Mason (Academic Press, New York).
24. Solid State Research Report, Lincoln Laboratory, M.I.T. (1965:3), p.43, DDC 629048.
25. Solid State Research Report, Lincoln Laboratory, M.I.T. (1965:2), p.60, DDC 624611, H-686.
26. D.H. Lyons and T.A. Kaplan, Phys. Rev. 120, 1580 (1960).
27. R. Plumier, J. de Physique (to be published).
28. Solid State Research Report, Lincoln Laboratory, M.I.T. (1965:3), p.45, DDC 629048.
29. Ibid., p. 47.
30. The calculation, based upon T. Oguchi, Phys. Rev. 117, 117 (1960), neglects kinematic interactions, and is valid to order (1/S) for Bravais lattices.
31. G. Shirane, et al., Phys. Rev. Letters 15, 146 (1965).
32. The neutron data were reinterpreted using a value of D_0 obtained from spin wave resonance experiments on iron, reported in T.G. Phillips, Phys. Letters 17, 11 (1965).
33. R. Weber and P.E. Tannenwald, Proceedings of the Eleventh Magnetism Conference, 1965 (J. Appl. Phys., to be published).
34. R. Weber and P.E. Tannenwald, private communication.

35. R.R. Birss, Rept. Progr. Phys. 26, 307 (1963); R.R. Birss, Symmetry and Magnetism (Wiley, New York, 1964).

36. W.H. Kleiner, Phys. Rev. 142, 318 (1966).

37. R.W. Terhune, P.D. Maker and C.M. Savage, Phys. Rev. Letters 14, 681 (1965).

38. L. Hall, Phys. Rev. 73, 775 (1948).

39. J. Morgan and B.E. Warren, J. Chem. Phys. 6, 666 (1938).

40. R.Y. Chiao, E. Garmire and C.H. Townes, Phys. Rev. Letters 13, 479 (1964).

41. P.L. Kelley, Phys. Rev. Letters 15, 1005 (1965), DDC 628563; Solid State Research Report, Lincoln Laboratory, M.I.T. (1965:3), p. 15, DDC 629048.

DOCUMENT CONTROL DATA – R&D

(Security classification of title, body of abstract and indexing annotation must be entered when the overall report is classified)

1. ORIGINATING ACTIVITY *(Corporate author)*
Lincoln Laboratory, M. I. T.

2a. REPORT SECURITY CLASSIFICATION
Unclassified

2b. GROUP
None

3. REPORT TITLE
Solid State Research

4. DESCRIPTIVE NOTES *(Type of report and inclusive dates)*
Quarterly Technical Summary – 1 November 1965 through 31 January 1966

5. AUTHOR(S) *(Last name, first name, initial)*
McWhorter, Alan L.

6. REPORT DATE	7a. TOTAL NO. OF PAGES	7b. NO. OF REFS
15 February 1966	80	93

8a. CONTRACT OR GRANT NO.	9a. ORIGINATOR'S REPORT NUMBER(S)
AF 19(628)-5167 b. PROJECT NO. 649L c. d.	Solid State Research (1966:1) 9b. OTHER REPORT NO(S) *(Any other numbers that may be assigned this report)* ESD-TR-66-42

10. AVAILABILITY/LIMITATION NOTICES
Distribution of this document is unlimited.

11. SUPPLEMENTARY NOTES	12. SPONSORING MILITARY ACTIVITY
None	Air Force Systems Command, USAF

13. ABSTRACT

This report covers in detail the solid state research work at Lincoln Laboratory for the period 1 November 1965 through 31 January 1966. The topics covered are Solid State Device Research, Optical Techniques and Devices, Materials Research, and Physics of Solids.

In order that four reports on solid state research may be issued during a calendar year, the number of this report is 1966 No. 1 rather than 1965 No. 4. There will be no report numbered 1965 No. 4.

14. KEY WORDS

electron beam pumping
solid state devices
solid state physics
laser research
materials research
hypersonic waves
optical pumping
impurity states
optical techniques and devices
cathodoluminescence
magnetism
infrared
photoelectron
electronic band structure
magnetoabsorption
microwave phonon generation
optical absorption
electroluminescence
magnetoreflection
magnetospectroscopy
magnetoplasma
stimulated Raman scattering